

Measurement and simulations of high-energy neutrons through a various thickness of concrete and steel shields using activation detectors at CHARM and CSBF

Noriaki Nakao, Toshiya Sanami, Tsuyoshi Kajimoto, Hiroshi Yashima, Robert Froeschl, Davide Bozzato, Elpida Iliopoulou, Angelo Infantino, Eunji Lee, Takahiro Oyama, Masayuki Hagiwara, Seiji Nagaguro, Tetsuro Matsumoto, Akihiko Masuda, Yoshitomo Uwamino, Arnaud Devienne, Fabio Pozzi, Marco Tisi, Tommaso Lorenzon, Nabil Mena, Heinz Vincke, Stefan Roesler & Markus Brugger

To cite this article: Noriaki Nakao, Toshiya Sanami, Tsuyoshi Kajimoto, Hiroshi Yashima, Robert Froeschl, Davide Bozzato, Elpida Iliopoulou, Angelo Infantino, Eunji Lee, Takahiro Oyama, Masayuki Hagiwara, Seiji Nagaguro, Tetsuro Matsumoto, Akihiko Masuda, Yoshitomo Uwamino, Arnaud Devienne, Fabio Pozzi, Marco Tisi, Tommaso Lorenzon, Nabil Mena, Heinz Vincke, Stefan Roesler & Markus Brugger (2024) Measurement and simulations of high-energy neutrons through a various thickness of concrete and steel shields using activation detectors at CHARM and CSBF, *Journal of Nuclear Science and Technology*, 61:4, 429-447, DOI: [10.1080/00223131.2023.2239243](https://doi.org/10.1080/00223131.2023.2239243)

To link to this article: <https://doi.org/10.1080/00223131.2023.2239243>



© 2023 The Author(s). Published by Informa UK Limited, trading as Taylor & Francis Group.



Published online: 13 Aug 2023.



[Submit your article to this journal](#)



Article views: 474



[View related articles](#)












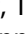




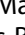


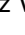

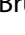



[View Crossmark data](#)



Citing articles: 1 [View citing articles](#)

Measurement and simulations of high-energy neutrons through a various thickness of concrete and steel shields using activation detectors at CHARM and CSBF

Noriaki Nakao ^a, Toshiya Sanami ^b, Tsuyoshi Kajimoto ^c, Hiroshi Yashima ^d, Robert Froeschl ^e, Davide Bozzato ^e, Elpida Iliopoulou ^e, Angelo Infantino ^e, Eunji Lee ^f, Takahiro Oyama ^b, Masayuki Hagiwara ^b, Seiji Nagaguro ^b, Tetsuro Matsumoto ^g, Akihiko Masuda ^g, Yoshitomo Uwamino ^a, Arnaud Devienne ^e, Fabio Pozzi ^e, Marco Tisi ^e, Tommaso Lorenzon ^e, Nabil Mena ^e, Heinz Vincke ^e, Stefan Roesler ^e and Markus Brugger ^e

^aShimizu Corporation, Institute of Technology, Tokyo, Japan; ^bRadiation Science Center, High Energy Accelerator Research Organization (KEK), Tsukuba, Ibaraki, Japan; ^cGraduate School of Advanced Science and Engineering, Hiroshima University, Hiroshima, Japan; ^dKyoto University Institute for Integrated Radiation and Nuclear Science (KURNS), Osaka, Japan; ^eRadiation Protection Group, CERN, Geneva, Switzerland; ^fDepartment of Applied Quantum Physics and Nuclear Engineering, Kyushu University, Fukuoka, Japan; ^gNational Metrology Institute of Japan (NMIJ), National Institute of Advanced Industrial Science and Technology (AIST), Ibaraki, Japan

ABSTRACT

A shielding experiment using activation detectors was performed at the CERN High-energy Accelerator Mixed-field (CHARM) facility and the CERN Shielding Benchmark Facility (CSBF). The protons (24 GeV/c) were bombarded into a 50-cm-thick copper target, and the released neutrons were transmitted through various shields located vertically upward from the target. Ordinary concrete slabs of 40- to 160-cm thicknesses and steel slabs of 20- to 80-cm thicknesses were installed by changing the material and the thickness of the shield. Activation detectors of bismuth, indium, aluminum, and graphite were variously placed in these shields and activated by high energy neutrons. From the radionuclide production rate in the activation detectors, the attenuation profiles through the various shielding materials were obtained for the reactions of $^{209}\text{Bi}(n,xn)^{210-x}\text{Bi}(x=4-9)$, $^{115}\text{In}(n,n')^{115m}\text{In}$, $^{27}\text{Al}(n,\alpha)^{24}\text{Na}$, and $^{12}\text{C}(n,2n)^{11}\text{C}$. Estimated attenuation lengths of high energy neutrons through concrete and steel were compared with cited data and discussed. Monte Carlo simulations using FLUKA, PHITS, and GEANT4 were also performed as benchmark calculations, and they agreed with the experimental data, generally within a factor of 2.

ARTICLE HISTORY

Received 24 April 2023
Accepted 18 July 2023

KEYWORDS



activation detector;
shielding; attenuation
length; benchmark; Monte
Carlo; FLUKA; PHITS; GEANT4

1. Introduction

Recently, a number of particle accelerator facilities have been constructed for physics research, medical irradiation, and industrial use. Accordingly, accelerator specifications have been upgraded to enhance the intensity and energy of the particle beam, providing better statistics of measurements and more efficient irradiation. To ensure the radiation safety in such facilities, the induced radioactivity and prompt radiation levels must be predicted from the data of secondary neutrons generated by beam irradiation. Because of the strong penetrability of produced neutrons, these accelerator facilities require massive shields to suppress the radiation levels outside the facility. As the radiation shield consumes a considerable portion of

the total construction costs, the shielding design is very important when constructing high-intensity, high-energy accelerator facilities.

Most of the conceptual shielding designs for high-energy accelerators are based on the point-kernel method. The method is subjected to not change the shape of neutron energy spectra on shield depth, namely, to form energy spectral equilibrium of neutrons in shields. The equilibrium occurs by higher energy neutrons producing lower energy neutrons by interactions in shields. During deep penetration through thick concrete shield, low energy neutrons below MeV region attenuate quickly; on the other hand, they are generated due to elastic and non-elastic scattering by the high-energy neutrons (approximately >20 MeV). Such phenomena cause

CONTACT Noriaki Nakao  noriaki.nakao@shimz.co.jp  Shimizu Corporation, Institute of Technology, 3-4-7, Etchujima, Koto-ku, Tokyo 135-8530, Japan

Present address for Elpida Iliopoulou is Hirslanden Private Hospital Group, Radiation Oncology Institute, Lausanne, Switzerland.

Present address for Eunji Lee is Radiation Science Center, High Energy Accelerator Research Organization (KEK), Tsukuba, Ibaraki, Japan.

Present address for Yoshitomo Uwamino is Japan Radioisotope Association, Tokyo, Japan.

Present address for Arnaud Devienne is ITER Delivery Department, Fusion For Energy, Barcelona, Spain.

Present address for Masayuki Hagiwara is Institute for Advanced Synchrotron Light Source, National Institutes for Quantum Science and Technology (QST), Sendai, Miyagi, Japan.

© 2023 The Author(s). Published by Informa UK Limited, trading as Taylor & Francis Group.

This is an Open Access article distributed under the terms of the Creative Commons Attribution-NonCommercial-NoDerivatives License (<http://creativecommons.org/licenses/by-nc-nd/4.0/>), which permits non-commercial re-use, distribution, and reproduction in any medium, provided the original work is properly cited, and is not altered, transformed, or built upon in any way. The terms on which this article has been published allow the posting of the Accepted Manuscript in a repository by the author(s) or with their consent.

neutrons to attain a spectral equilibrium state; therefore, the attenuation curve is strongly ruled by high-energy neutrons. For instance, the Moyer model [1] assumes that the dose rate of neutrons in a spectral equilibrium state behind the thick concrete shield is exponentially attenuated.

The Moyer model computes the dose rate behind the shield at various angles arising from prompt radiations by a beam loss at a point or a line source. However, this model is often used for the dose rate evaluation, especially at a point perpendicular (90°) to the beam direction due to a point beam loss. In this case, the dose rate H [mSv/h] is expressed as follows:

$$H = JH_1 \frac{1}{r^2} \exp\left(-\frac{d\rho}{\lambda}\right), \quad (1)$$

where J [W] is the beam loss power at the source point, H_1 [(mSv/h) cm²/W] is dose rate at 1-cm distance for a unit beam-loss power, r [cm] is the distance between the beam-loss point and the estimation point, and d [cm] is the effective shield thickness. ρ [g/cm³] is the density of the shielding material and λ [g/cm²] is the attenuation length. Tesch et al. also proposed the equation of the dose rate at 90° direction for the point beam loss [2], which is almost identical to the Eq. (1), where H_{casc} corresponds to H_1 . Where, the H_{casc} parameters were summarized based on the experimental data for neutron yields from various targets that were bombarded with protons of energies up to about 1 GeV, and the λ values based on the experiment were also summarized for the lateral concrete shield [2].

The attenuation lengths of thick lateral shields have been measured at several accelerator facilities. Stevenson et al. measured for the earth around the proton synchrotron (PS) in the Conseil Européen pour la Recherche Nucléaire (CERN) at energies of 13.7 and 25.5 GeV [3]. Ban et al. measured the neutron attenuation length in concrete for 12-GeV and 500-MeV proton beams at High Energy Accelerator Research Organization (KEK) [4,5]. At Los Alamos Neutron Science Center (LANSCE) facility of Los Alamos National Laboratory (LANL), Bull et al. measured the neutron spectra behind a lateral steel shield using 800-MeV proton beam and the attenuation length for steel was experimentally evaluated [6]. At the ISIS spallation-neutron source facility using 800-MeV proton beam in the Rutherford Appleton Laboratory (RAL), Nunomiya et al. measured the attenuation lengths of concrete and iron for the neutrons in lateral direction [7]. At the Alternating Gradient Synchrotron (AGS) in Brookhaven National Laboratory (BNL), a shielding experiment with a mercury spallation target bombarded with 24-GeV protons was performed, and attenuation lengths for concrete and iron were experimentally evaluated [8]. In Fermi National Accelerator Laboratory (FNAL), a shielding experiment with iron

and concrete was performed with a beryllium target irradiated by 120-GeV protons at the Pbar target station, and the neutron attenuation length was evaluated [9]. However, such reliable experiments are scarcely reported, and their results are dispersed mainly because of the difference in complex experimental geometry.

Several other experiments, which were not the direct measurement of attenuation length, were conducted on neutron penetration using typical shielding materials at high-energy proton accelerator facilities. In the Takasaki Ion Accelerators for Advanced Radiation Application (TIARA) of the Japan Atomic Energy Research Institute (JAERI, currently the National Institutes for Quantum and Radiological Science and Technology), 40- and 65-MeV quasi-monoenergetic neutrons were produced by proton beams, and the neutron energy spectra were measured behind concrete [10], iron [11], and polyethylene [12] shields. At the KEK spallation neutron source (KENS) facility using 500-MeV proton beam, the attenuation of neutrons in forward direction through the concrete shield was measured [13]. In the CERN-EU High Energy Reference Field (CERF) facility, a 120-GeV/c positive-hadron beam was directed at a thick copper target, and the neutron energy spectra between 32 and 380 MeV were measured behind the lateral shields of concrete and iron [14]. Recent shielding designs for high energy particle facilities are performed using Monte Carlo simulations to predict prompt and residual radiation level inside and outside facilities. To validate the database and algorithms in theoretical simulation programs, experimental data are indispensable. The results above mentioned benchmark experiments have been widely used in validations of nuclear models, parameters, and reaction cross-sections in various radiation simulation codes.

The CERN High-energy Accelerator Mixed-field (CHARM) facility [15,16] is suitable to experiments on radiation shielding because of simple shield constructions. In 2015, our experimental team performed a deep-penetration shielding experiment for radiation shielding design of high energy accelerators [17–20]. High-energy (24 GeV/c) protons were injected into a 50-cm-thick copper target, generating neutrons that penetrated a bulk shield of a 360 cm-thick concrete placed vertically upward from the target. The neutrons transmitted through the concrete of various thicknesses were measured using bismuth and aluminum activation detectors placed inside the shield, and the neutron attenuation length for lateral concrete shield was estimated and compared with the Monte Carlo simulations [17]. In 2016, the shield structure of the top roof of the CHARM facility was changed and the two experimental areas were arranged in the vertical shield, collectively denoted as CERN Shielding Benchmark Facility (CSBF). In this report, a shielding

experiment with activation detectors using the newly changed shield setups of the CSBF facility and comparisons between experimental and simulated results are described in detail. Attenuation lengths evaluated from this experiment are also discussed and compared with the cited data.

2. Experiment

2.1. Facility and experimental set up

Figures 1 and 2 show the horizontal and vertical cross-sections, respectively, at the beam-axis of the CHARM facility in the east hall at CERN. The 24-GeV/c

protons are transported from the PS and are transmitted through the proton IRRADIATION facility (IRRAD) [21], a reference proton irradiation facility built for characterizing detector elements and other accelerator components against radiation, and are finally injected into a target located at the center of the CHARM facility. One of the different irradiation targets can be selected by revolving the four target holders as shown in Figure 1. The irradiation targets are copper, aluminum, and aluminum with many tiny holes like a sieve. All targets are 8 cm in diameter and 50 cm in thickness. The fourth target holder is left empty as a blank. The copper target was selected for the shielding experiment. The protons not stopped at

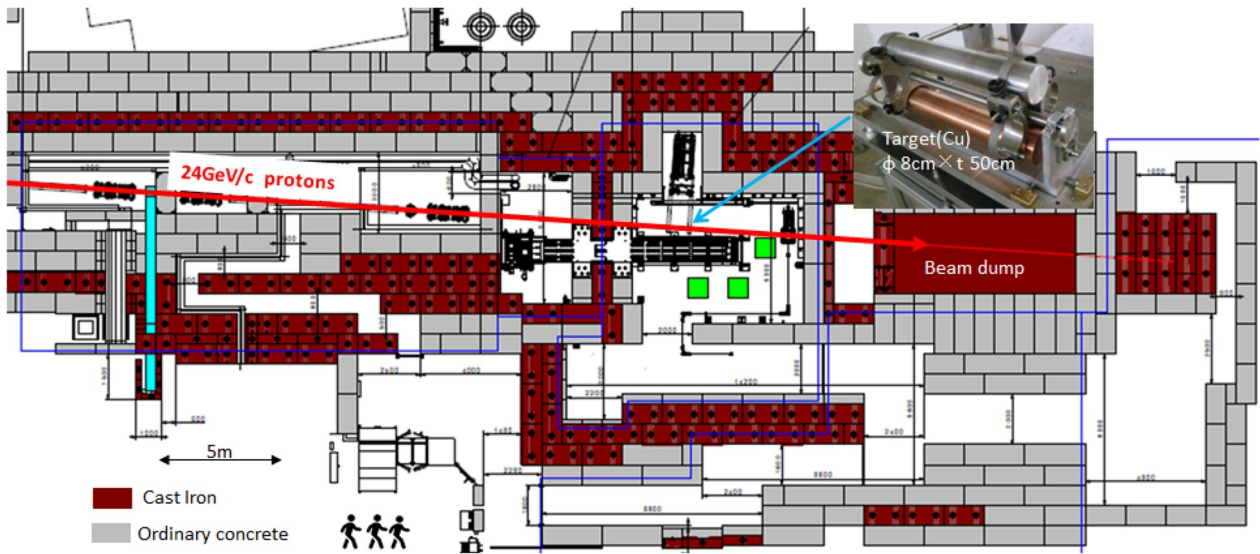


Figure 1. Horizontal cross-section at the beam-axis height of the CHARM facility.

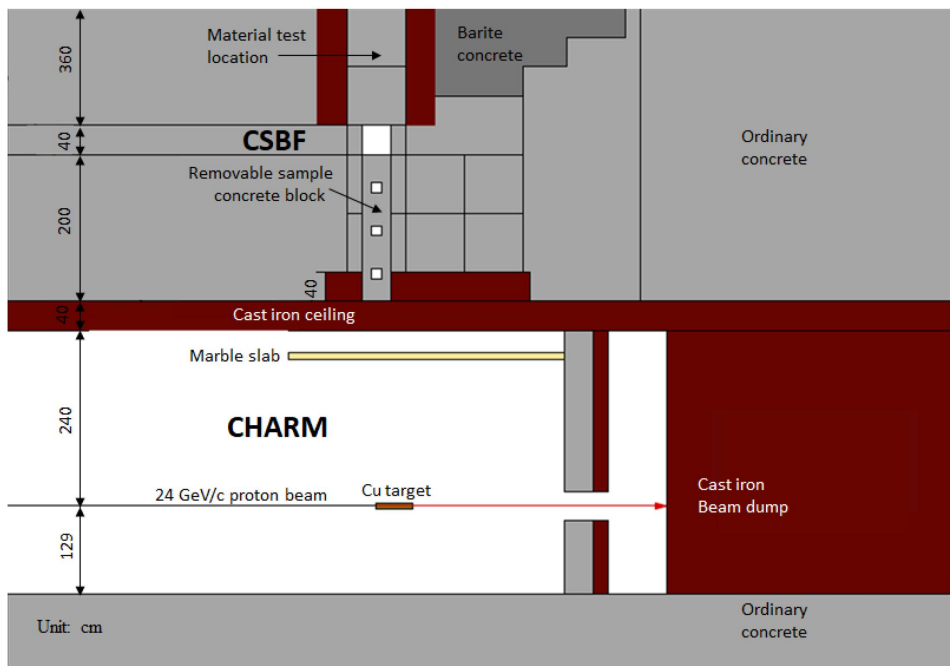


Figure 2. Vertical cross-section at the beam-axis plane of the CHARM and CSBF facilities which are below and above the cast iron ceiling, respectively.

the target are transported into the iron beam dump placed in the downstream. The proton beam line and the target room are surrounded by concrete and cast-iron shielding, and the target room can only be accessed through the maze corridor.

Figure 3 shows the vertical cross-section of the CHARM facility and the CSBF, which is perpendicular to the beam-axis at the target location. The target center is positioned on the beam-axis, which is 129 cm above the floor. To the right of the target in Figure 3, there is a four-layered movable shield wall of steel and concrete. Each of the shield layer is 20-cm in thickness and 214-cm in height from the floor. The movable shield was fully inserted to the target room during irradiations in this experiment as shown in Figure 1. Above the ceiling of the target room, located 240 cm above the beam line, a bulk shield consists of 80-cm-thick cast iron and 360-cm-thick ordinary concrete. A 10-cm-thick marble ceiling is installed at 185 cm above the beam line.

In 2016, the shield structure of the top roof of the CHARM facility was changed, and two shielding experimental areas in CSBF were arranged as shown in Figures 2 and 3. One has a space of 40-cm and 40-cm plane and 240-cm depth, and the bottom face was 40-cm cast iron slab just above the target room ceiling, which was 240 cm above from the beam line. We can insert a removable sample concrete block (hereafter, removable block) in the space. The removable block has 37-cm by 37-cm plane, 200-cm length, and three holes to place activation samples. Figure 4 shows the photos of the removable block which is installed into this space. The other experimental area was a material test location (80-cm by 80-cm plane, 160-cm depth) located above the space for the removable block. In the material test location, ordinary concrete slabs of 40- to

160-cm thicknesses or steel slabs of 20- to 80-cm thicknesses were installed as shown in Figure 5, changing the materials and the thicknesses to measure neutron flux of the various settings.

Compositions and densities of the materials are listed in Table 1. The concrete composition and the density of the bulk shield are derived from CERN-wide measurements on typical shielding blocks [14], while the density of the blocks specifically used for the test shield was measured in 2022. The shielding experiments were carried out for four periods in 2016, 2017, 2018, and 2022; the shield layouts in each experiment are shown in Figure 6. Table 2 lists the detail of all irradiations including irradiation durations, shield types, and sizes of the activation detector samples.

2.2. Activation detector samples

The neutrons transmitted through the various shield settings were estimated by observing activation reactions of the detector samples composed of bismuth, indium, aluminum, and graphite (see Figure 7), which are widely used in high-energy neutron measurements [7,13,22]. The samples were each prepared in three sizes (8.0 cm dia. \times 1.0 cm thick, 4.0 cm dia. \times 0.4 cm thick and 2.0 cm dia. \times 0.2 cm thick). The sample size was varied because the neutron intensity varies due to the shielding settings. As shown in Figures 4, 6(a-b), the samples were placed at four locations (3 holes and the top of the removable block). On the other hand, as shown in Figures 5 and 6, samples were placed upon the various test shield settings in the material test location. Samples were also placed on the lower side of the shield surface for the irradiation of the 0-cm thickness.

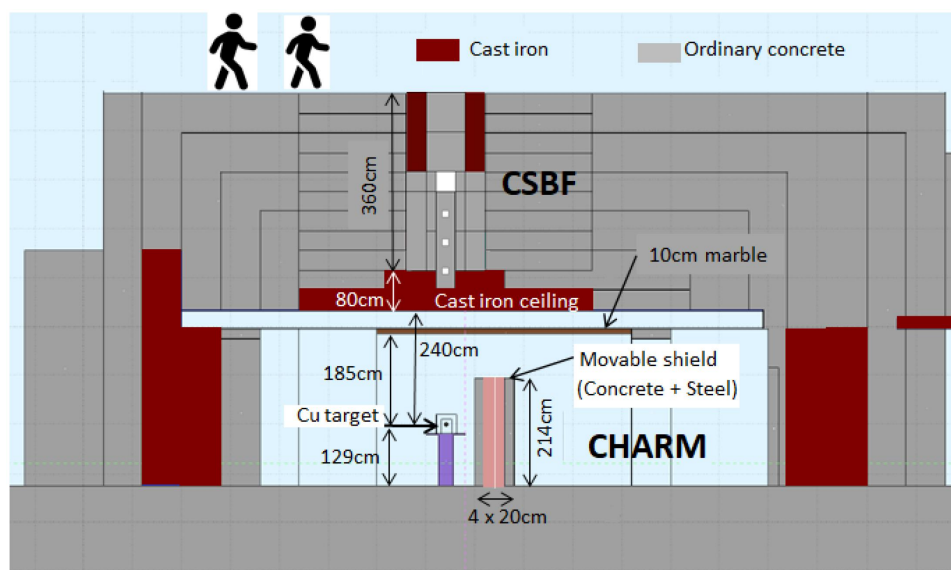


Figure 3. Vertical cross-section of the CHARM and CSBF facilities (below and above the cast iron ceiling, respectively) perpendicular to the beam-axis at the target location. The beam travels from front to back of this figure.

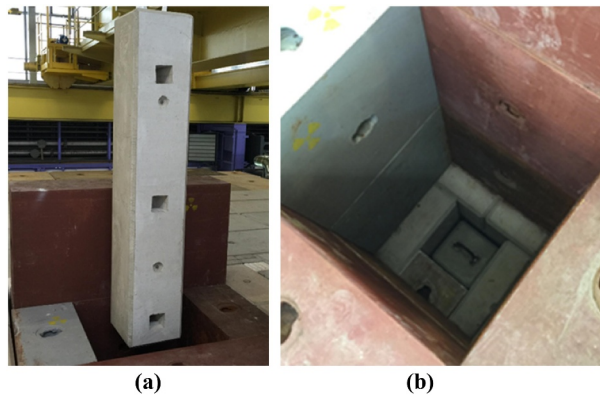


Figure 4. Photographs of (a) whole removable block and (b) that installed into the collimator.

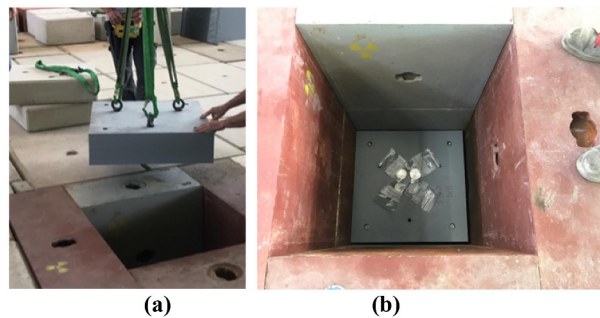


Figure 5. Photographs of (a) crane work for installing steel test shield and (b) the samples on it at the material test location.

Table 1. Density and chemical composition of the materials used in the present experiment.

Material Density [g/cm ³]	Element	Weight [%]	Element	Weight [%]
Ordinary Concrete	H	0.561	Si	16.175
	C	4.377	S	0.414
	O	48.204	K	0.833
2.4 (Bulk shield)	Na	0.446	Ca	23.929
2.23 (Test shield)	Mg	1.512	Ti	0.173
	Al	2.113	Fe	1.263
Steel 7.77	Fe	98.34	P	0.045
	C	0.17	S	0.045
	Mn	1.40		
Barite Concrete 3.35	H	0.358	S	10.703
	O	31.162	Ca	4.966
	Mg	0.120	Fe	4.737
	Si	1.046	Ba	46.339
Cast Iron 7.2	Al	0.418		
	Fe	92.3	P	0.08
	C	3.85	S	0.02
	Mn	0.3	Co	0.05
Marble 2.71	Si	3.4		
	Ca	40.0	O	48.0
Movable Shield (Steel S235JR) 7.85	C	12.0		
	Fe	97.793	P	0.035
	C	0.17	S	0.035
	Mn	1.4	N	0.012
	Cu	0.55	Co	0.005

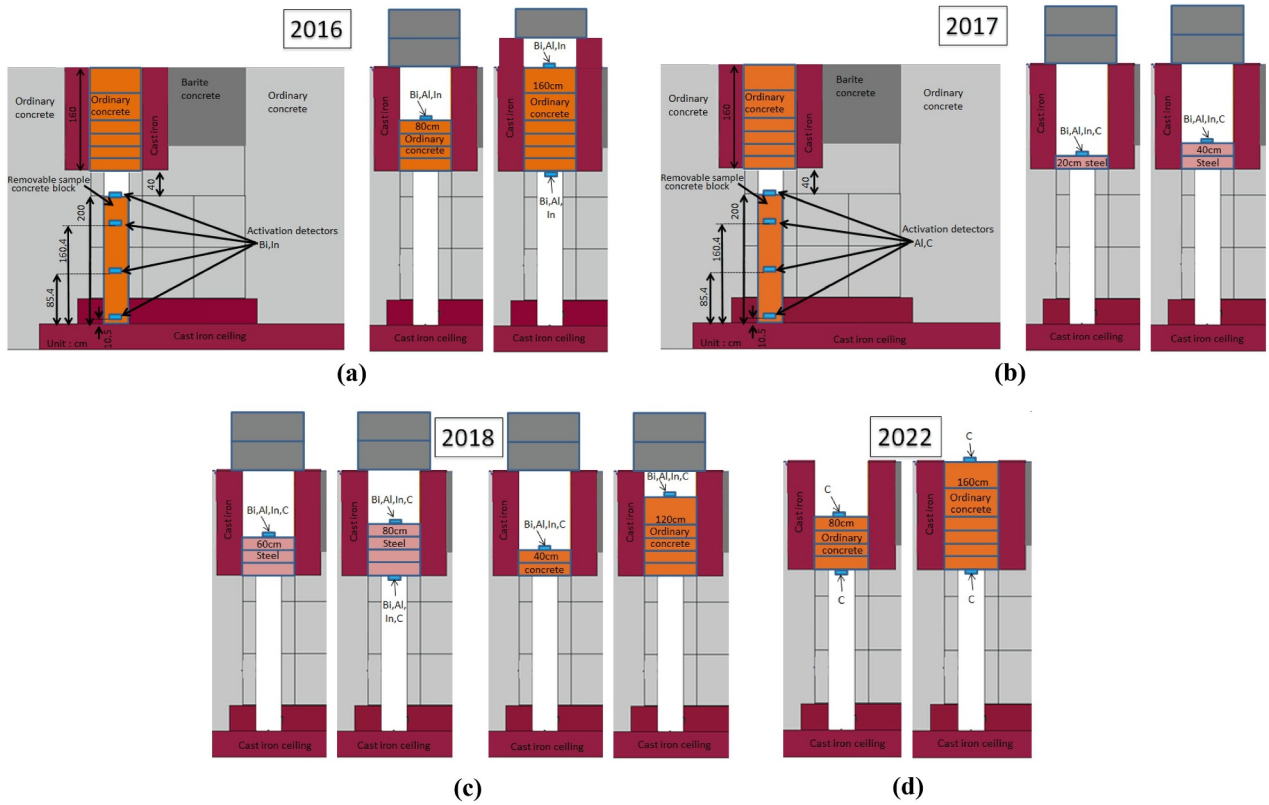


Figure 6. Vertical cross-section of the configurations at the CSBF experiment in (a) 2016, (b) 2017, (c) 2018 and (d) 2022.

2.3. Beam irradiation

The maximum design intensity of the 24-GeV/c proton beam from the PS is 5×10^{11} protons per pulse, where the pulse length is 350 ms. The beam pulses are distributed to multiple beam lines, and the maximum average design intensity at CHARM is 6.7×10^{10} proton/s (p/s) [23]. The spill-by-spill beam intensity is monitored by a Secondary Emission Chamber (SEC) [24], which is calibrated using the aluminum activation method [25]. Figure 8 exemplifies the average intensity history measured with the SEC monitor during the shielding experiment in 2017. The SEC monitor is located before IRRAD, approximately 23.4 m upstream of the CHARM target. The average intensity ranged from 0.5×10^{10} to 4.0×10^{10} p/s. The irradiation durations are listed in Table 2. After the irradiation period, the beam was temporarily stopped to remove the irradiated samples and install new samples at the different shielding setting.

2.4. Radioactivity measurements

The removed samples were transported to the locations of high-purity germanium-semiconductor (HPGe) detectors, and the energy spectra of the photons from the radionuclides generated in the samples by the $^{209}\text{Bi}(n,xn)^{210-x}\text{Bi}(x=4-9)$, $^{115}\text{In}(n,n')^{115m}\text{In}$, $^{27}\text{Al}(n,\alpha)^{24}\text{Na}$, and $^{12}\text{C}(n,2n)^{11}\text{C}$ reactions were measured.

To estimate the radioactivities of the nuclides with short (^{201}Bi and ^{202}Bi), medium (^{203}Bi and ^{204}Bi), and long (^{205}Bi and ^{206}Bi) half-lives, the bismuth samples

were measured continuously three times with the measurement times of approximately 3, 15, and 24 hours. The aluminum samples were measured at times between 3 and 24 hours, depending on the peak count rates of the photons from ^{24}Na . For others, measuring times were 4 hours for the indium and 15–30 minutes for the graphite samples.

2.5. Data analysis

Table 3 lists the analyzed radionuclide production reactions, half-lives, and photon energies with their emission ratios. Figure 9 shows all photo-peaks in the measured energy spectra of the photons emitted from radionuclides. The net counts of the photo-peaks at the corresponding photon energies were obtained by summing the counts of peak regions and subtracting the baseline contribution, which was estimated at both sides of the peak as shown in Figure 9. The peak counts S and their standard deviations σ were respectively estimated as follows:

$$S = N_p - \beta_1 N_1 - \beta_2 N_2 \quad (2)$$

$$\sigma = \sqrt{N_p + \beta_1^2 N_1 + \beta_2^2 N_2} \quad (3)$$

where $\beta_1 = 0.5W_p/W_1$ and $\beta_2 = 0.5W_p/W_2$. N_p , N_1 , and N_2 are the gross counts of the peak region, baseline region 1 and baseline region 2, respectively, while W_p , W_1 , and W_2 are the corresponding channel widths.

Table 2. Irradiation durations, shield types, and sizes of the activation detector samples.

Irradiation			Shield			Sample		
Year Month	Date & Time		Type	Material	Thickness [cm]	Name	Diameter [cm]	Thickness [cm]
	Start	Stop						
2016 September	16th 1:30	20th 15:00	Removable sample block	Concrete	200.0	Bi-823	8.0	1.0
					160.4	Bi-813	8.0	1.0
					85.4	Bi-402	4.0	0.4
					10.5	Bi-215	2.0	0.2
					10.5	Bi-215	2.0	0.2
	21st 13:00	22nd 9:00	Removable sample block	Concrete	200.0	In-802	8.0	1.0
					160.4	In-801	8.0	1.0
					85.4	In-401	4.0	0.4
					10.5	In-251	2.0	0.2
					10.5	In-251	2.0	0.2
	22nd 11:50	23rd 8:30	Material test location	Concrete	0.0	Bi-405	4.0	0.4
					0.0	Al-405	4.0	0.4
					0.0	In-255	2.0	0.2
	22nd 17:30		Material test location	Concrete	160.0	Bi-814	8.0	1.0
					160.0	Al-804	8.0	1.0
					160.0	In-804	8.0	1.0
	26th 17:40	27th 8:50	Material test location	Concrete	80.0	Bi-835	8.0	1.0
					80.0	Al-805	8.0	1.0
80.0					In-805	8.0	1.0	
2017 August	23rd 12:30	23rd 11:30	Removable sample block	Concrete	200.0	C-804	8.0	1.0
					85.4	C-802	8.0	1.0
					10.5	C-402	4.0	0.4
					10.5	C-402	4.0	0.4
					10.5	C-402	4.0	0.4
	23rd 13:55	23rd 15:00	Removable sample block	Concrete	160.4	C-803	8.0	1.0
					10.5	C-801	8.0	1.0
					10.5	C-401	4.0	0.4
					10.5	C-401	4.0	0.4
					10.5	C-401	4.0	0.4
	23rd 15:35	24th 6:00	Removable sample block	Concrete	200.0	Al-811	8.0	1.0
					160.4	Al-810	8.0	1.0
					85.4	Al-809	8.0	1.0
					10.5	Al-409	4.0	0.4
					10.5	Al-808	8.0	1.0
	24th 17:45	25th 8:30	Material test location	Steel	20.0	Bi-816	8.0	1.0
					20.0	In-806	8.0	1.0
					20.0	Al-806	8.0	1.0
20.0					C-806	8.0	1.0	
20.0					C-806	8.0	1.0	
28th 17:10	29th 8:30	Material test location	Steel	40.0	Bi-817	8.0	1.0	
				40.0	In-807	8.0	1.0	
				40.0	Al-807	8.0	1.0	
				40.0	Al-807	8.0	1.0	
				40.0	C-807	8.0	1.0	
2018 August	22nd 21:00	23rd 9:00	Material test location	Steel	0.0	Bi-415	4.0	0.4
					0.0	In-415	4.0	0.4
					0.0	Al-415	4.0	0.4
					0.0	C-415	4.0	0.4
					0.0	C-815	8.0	1.0
					80.0	Bi-838	8.0	1.0
					80.0	In-808	8.0	1.0
					80.0	Al-818	8.0	1.0
					80.0	C-818	8.0	1.0
					80.0	C-818	8.0	1.0
	23rd 18:30	24th 8:45	Material test location	Steel	60.0	Bi-837	8.0	1.0
					60.0	In-807	8.0	1.0
					60.0	Al-817	8.0	1.0
	27th 17:20	28th 8:40	Material test location	Concrete	120.0	C-817	8.0	1.0
					120.0	Bi-840	8.0	1.0
					120.0	In-810	8.0	1.0
					120.0	Al-820	8.0	1.0
					120.0	C-820	8.0	1.0
28th 18:40	29th 3:00	Material test location	Concrete	40.0	Bi-839	8.0	1.0	
				40.0	In-809	8.0	1.0	
				40.0	Al-819	8.0	1.0	
				40.0	Al-819	8.0	1.0	
				40.0	C-819	8.0	1.0	
2022 August	26th 9:25	26th 10:30	Material test location	Concrete	80.0	C-803	8.0	1.0
	26th 10:51	26th 11:50	Material test location	Concrete	160.0	C-806	8.0	1.0
	26th 9:25	26th 13:15	Material test location	Concrete	0.0	C-801	8.0	1.0

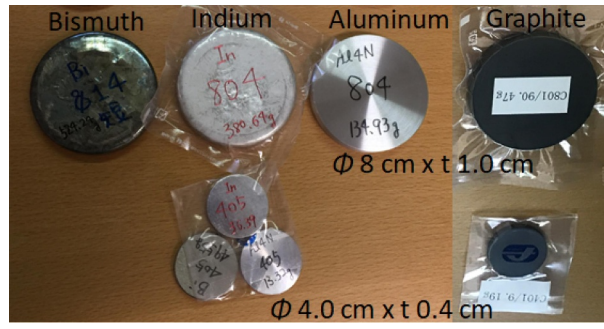


Figure 7. Photographs of the activation-detector samples of bismuth, indium, aluminum and graphite.

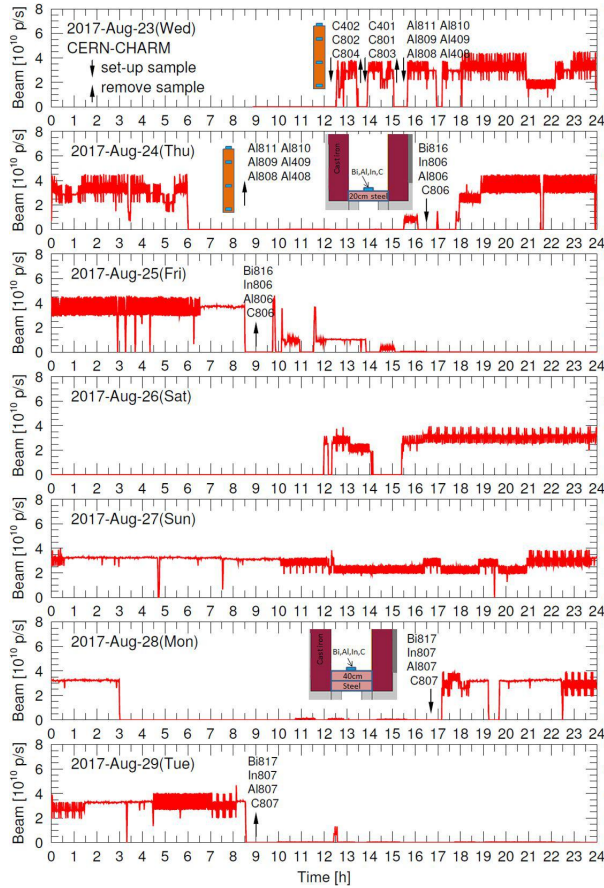


Figure 8. History of irradiated beam intensity in 2017.

Finally, the production rates R [number/atom/proton] in the activation-detector samples were estimated with the detector efficiencies and the beam intensity fluctuations during the irradiation.

$$R = \frac{S\lambda_d}{AN\epsilon\gamma} \quad (4)$$

where

$$A = \sum_{i=1}^n \left\{ \frac{Q_i}{\Delta t} (1 - e^{-\lambda_d \Delta t}) e^{-\lambda_d (n-i) \Delta t} \right\} e^{-\lambda_d T_c} (1 - e^{-\lambda_d T_m}),$$

and S is the peak count, λ_d is the decay constant of the radionuclide [min^{-1}], N is the number of atoms in the activation-detector sample. γ is the emission ratio, n is the total number of time bins

in the beam-history data, Q_i is the number of protons in the i -th time bin, and Δt is the width of the time bin in the beam-history data [min]. T_c and T_m denote the cooling and measuring times, respectively [both in min]. ϵ is the photo-peak efficiency of the HPGe detector, estimated by using the LabSOCS software (Mirion Technologies Canberra KK) [26].

The neutron attenuation through the thick activation detector was also taken into account, and the correction factors were estimated by Monte Carlo simulations with using Particle and Heavy Ion Transport code System (PHITS) Ver-3.24 [27] and Electron Gamma Shower Version 5 (EGS5) [28].

Table 3. Production reactions, half-lives, and photon energies of the radionuclides in the activation detectors.

Reaction	Half Life	Photon Energy [keV] (Emission Ratio)	
$^{115}\text{In}(n,n')^{115\text{m}}\text{In}$	4.486 h	336.0 (0.458)	
$^{27}\text{Al}(n,\alpha)^{24}\text{Na}$	14.96 h	1368.6 (1.000)	2754.6 (0.999)
$^{12}\text{C}(n,2n)^{11}\text{C}$	20.39 min	511.0 (1.995)	
$^{209}\text{Bi}(n,4n)^{206}\text{Bi}$	6.24 d	803.1 (0.989)	1718.7 (0.318)
$^{209}\text{Bi}(n,5n)^{205}\text{Bi}$	15.31 d	703.4 (0.310)	1764.4 (0.325)
$^{209}\text{Bi}(n,6n)^{204}\text{Bi}$	11.22 h	899.2 (0.988)	984.0 (0.593)
$^{209}\text{Bi}(n,7n)^{203}\text{Bi}$	11.76 h	820.2 (0.297)	825.3 (0.146)
$^{209}\text{Bi}(n,8n)^{202}\text{Bi}$	1.72 h	422.2 (0.837)	657.5 (0.606)
$^{209}\text{Bi}(n,9n)^{201}\text{Bi}$	1.80 h	629.1 (0.240)	960.7 (0.994)

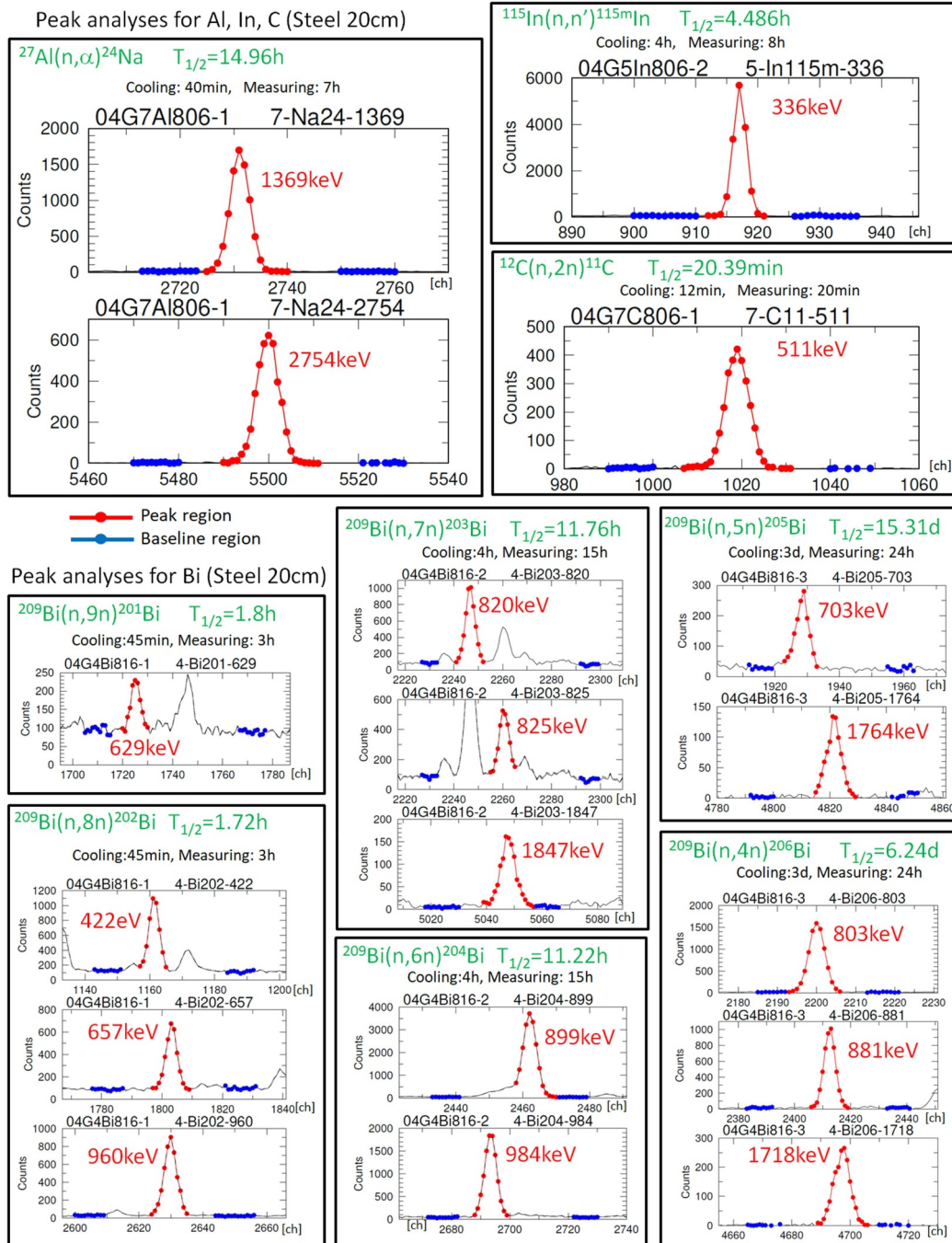


Figure 9. Analyzed all photo-peaks and base-line regions in the energy spectra of gamma-rays from radionuclides measured by the HPGe-detector.

3. Monte Carlo simulations

Monte Carlo simulations were performed with FLUctuating KAskade code (FLUKA) v4-2.2 distributed by the FLUKA.CERN collaboration [29,30] and PHITS Ver-3.24 [27] and GEometry ANd Tracking (GEANT) ver.4.10.07-02 [31,32] to compare with the experimental data for benchmarking. In the PHITS calculation, the JENDL-4.0 data library [33] for neutrons below 20 MeV, the evaporation model GEM [34] for the neutrons above 20 MeV and protons, the intra-nuclear cascade model INCL [35] for neutrons up to 3 GeV, and the JAM model [36] for nuclear reaction above 3 GeV were used. The physics list FTFP_BERT_HP was used in the GEANT4 simulation [37]. The geometry of the CSBF experimental set up was included in the calculations. The primary source considered is a 24-GeV/c proton beam having a gaussian spatial profile with a FWHM of approximately 1.2 cm in the transverse plane with respect to the beam direction.

As already detailed in the previous sections, the number of protons that reach the target at CHARM is monitored using a SEC, which is located before IRRAD (approximately 23.4 m upstream of the CHARM target). In the FLUKA simulations, the origin point of the primary source corresponded to the position of the secondary emission chamber. This allowed to take into account the beam profile dispersion due to both the air path before the CHARM target and the possible interaction with thin electronic components, such as

silicon sensors, that may be present in IRRAD during operation for irradiation studies. Dedicated FLUKA calculations were performed to estimate this dispersion considering the air path and various equivalent silicon thickness: the energy integrated neutron fluence outside the CHARM target and at a point perpendicular (90°) to the beam direction for each case analyzed was compared to the case in which the beam is assumed to start right in front of the target itself. As shown in Figure 10, for small thicknesses, the reduction factors scale linearly with the equivalent silicon thickness: considering the exact irradiation conditions of the experiments described in the present work, the correction factor to be applied if the beam is assumed to start right before the target is approximately 0.925. All the FLUKA calculations were performed with 60 CPUs in the CERN calculation cluster system.

For the PHITS and GEANT4 simulations, the source started from the beam entrance of the CHARM irradiation room. Therefore, the source intensity was multiplied by 0.925 as described above. Track-length estimator was used for scoring the particle in the detector regions to estimate particle fluxes. The calculations were performed with more than 50 CPUs.

For all simulations, energy spectra of scored particles were estimated starting from thermal energy for FLUKA, above 0.1 MeV for PHITS and above 0.315 MeV for GEANT4 calculations. Produced radionuclides were obtained by folding the energy spectra with the reaction cross-sections [38], as shown in Figure 11.

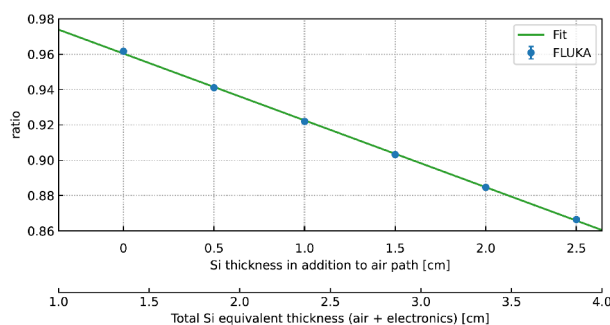


Figure 10. Estimation of correction factors to account for the beam dispersion in the case it is assumed in the Monte Carlo simulations that the primary beam starts right in front of the CHARM target instead of upstream IRRAD.

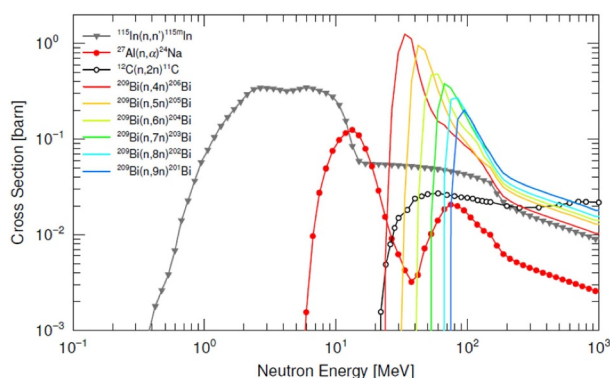


Figure 11. Reaction cross sections of radioactive nuclide production for the activation detectors.

4. Results and discussion

4.1. Experimental attenuation lengths

The measured production rates of all radionuclides for the removable block, concrete, and steel shields are shown in Figures 12, 13, and 14, and the numerical data are listed in Tables 4, 5, and 6, respectively. The errors of radionuclide production rates in the figures and tables are the statistical errors of the gamma-ray counting, but the uncertainties in the Ge-detector efficiency by LabSOCS (4.3%) [26] and the beam-intensity-monitor calibration (7%) [18] were not included. Table 7 summarizes all the uncertainties.

From the experimental attenuation curves, the attenuation lengths for all radionuclides were obtained by data-fitting of Equation (1), with experimental data excluding the thinnest points where the neutron spectra are not yet in equilibrium state. The fitted curves are also shown together with the experimental data in Figures 12, 13, and 14, and the attenuation lengths for all radionuclides in the removable block, concrete, and steel shields are plotted in Figure 15. As the measured radionuclide production rates have comparatively large statistical errors, the attenuation lengths were dispersed. Finally, the experimental attenuation lengths were obtained by averaging all data and are also shown in the figures with the standard deviation.

The obtained attenuation lengths through the concrete and steel in this experiment are compared with those of the cited experiments in high-energy accelerator facilities with proton energies above 10 GeV as listed in Table 8. For concrete shield, two experimental attenuation lengths obtained in this work gave a discrepancy probably because of the structure difference of the surrounding shield. For example, the attenuation length for the concrete in the material test location was smaller, which means quicker attenuation than that for the removable block because the cast iron around the test location absorbed and scattered neutrons. On the other hand, there is an agreement within error between lengths by us and Lee et al., who measured for concrete in the test location at the same facility but by using a different detector type in the different location [39]. The attenuation length for concrete obtained with the CHARM original bulk shield by Nakao et al. [17], which was an ideal experimental condition with the wide and simple shield structure, was $120 \pm 7 \text{ g/cm}^2$, which agreed with that by Stevenson et al. [3], but they are longer than those in this work. The attenuation lengths for concrete by Ban et al. [4] and by Nakashima et al. [8] gave much longer and shorter, respectively, than other experimental results.

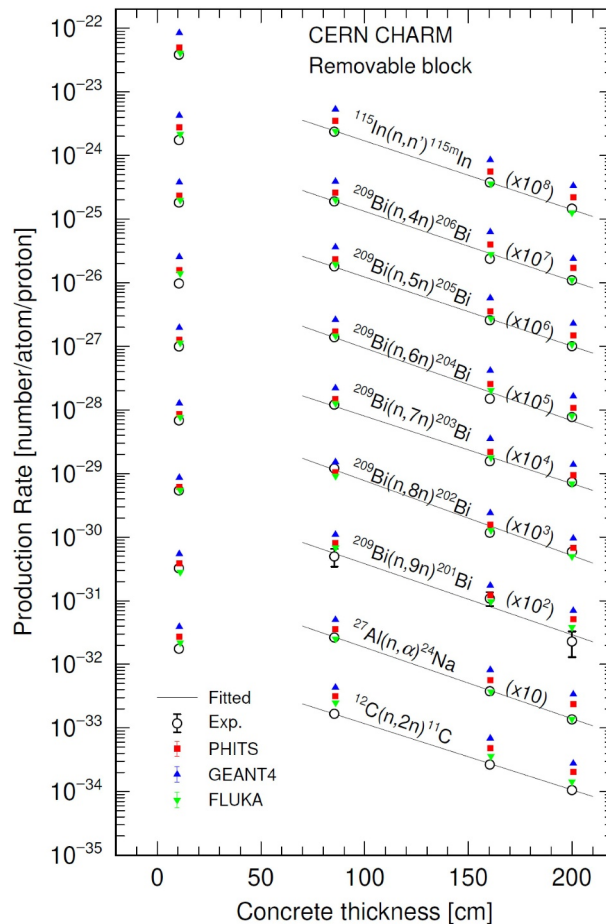


Figure 12. Attenuation profiles of the radionuclide production rates in the removable block.

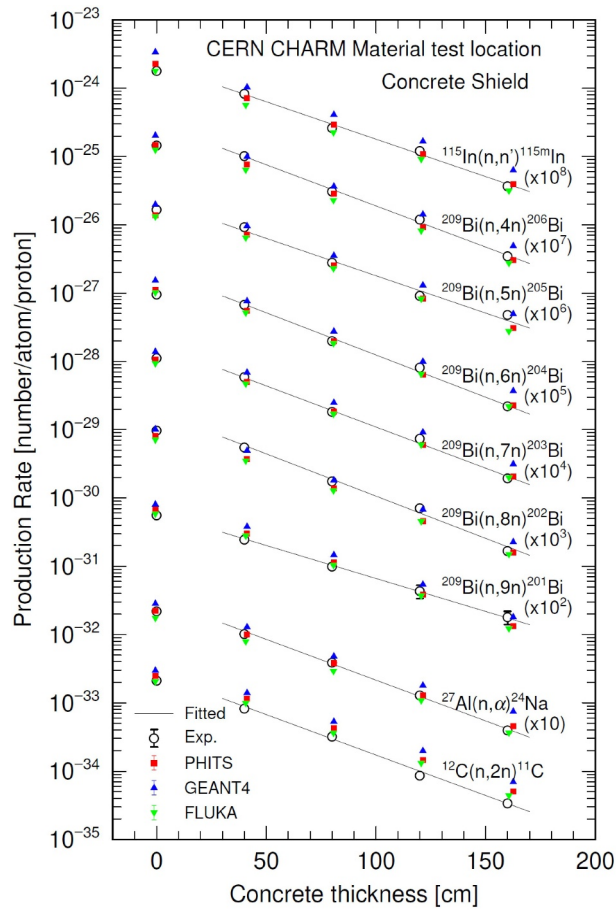


Figure 13. Attenuation profiles of the radionuclide production rates in the concrete shield at material test location.

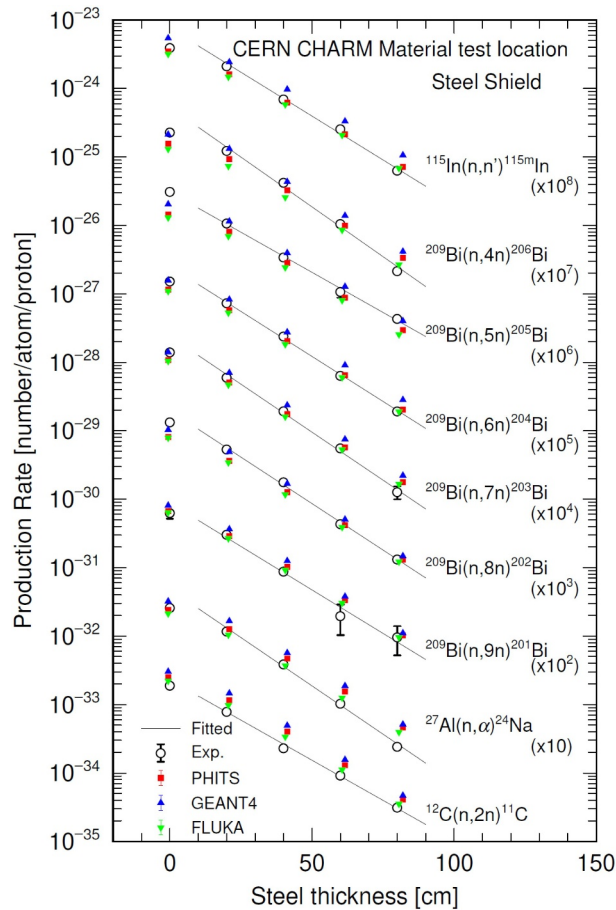


Figure 14. Attenuation profiles of the radionuclide production rates in the steel shield at material test location.

Table 4. Measured and simulated radionuclide production rates and C/E's in the removable block.

	Thickness [cm]	Experiment	FLUKA		PHITS		GEANT4	
		[1/atom/p] (Err%*)	[1/atom/p] (Err%)	C/E(AbsErr**)	[1/atom/p] (Err%)	C/E(AbsErr)	[1/atom/p] (Err%)	C/E(AbsErr)
^{115m} In	10.5	3.87×10 ⁻³¹ (7.2%)	4.09×10 ⁻³¹ (0.43%)	1.06 (0.08)	4.99×10 ⁻³¹ (0.14%)	1.29 (0.09)	4.88×10 ⁻³¹ (0.16%)	2.19 (0.16)
	85.4	2.38×10 ⁻³² (1.3%)	2.41×10 ⁻³² (0.60%)	1.01 (0.01)	3.52×10 ⁻³² (0.51%)	1.48 (0.02)	5.34×10 ⁻³² (0.63%)	2.25 (0.03)
	160.4	3.80×10 ⁻³³ (7.0%)	3.59×10 ⁻³³ (0.87%)	0.94 (0.07)	5.62×10 ⁻³³ (1.28%)	1.48 (0.11)	8.54×10 ⁻³³ (1.59%)	2.25 (0.16)
	200.0	1.47×10 ⁻³³ (4.5%)	1.26×10 ⁻³³ (1.08%)	0.86 (0.04)	2.21×10 ⁻³³ (2.05%)	1.50 (0.07)	3.35×10 ⁻³³ (2.71%)	2.28 (0.12)
²⁴ Na	10.5	3.26×10 ⁻³² (1.5%)	2.81×10 ⁻³² (0.80%)	0.86 (0.01)	3.87×10 ⁻³² (0.24%)	1.19 (0.02)	5.46×10 ⁻³² (0.30%)	1.67 (0.03)
	85.4	2.66×10 ⁻³³ (2.3%)	2.52×10 ⁻³³ (0.82%)	0.95 (0.02)	3.58×10 ⁻³³ (0.72%)	1.35 (0.03)	5.04×10 ⁻³³ (0.93%)	1.89 (0.05)
	160.4	3.80×10 ⁻³⁴ (3.4%)	3.70×10 ⁻³⁴ (1.25%)	0.97 (0.04)	5.65×10 ⁻³⁴ (1.84%)	1.49 (0.06)	8.23×10 ⁻³⁴ (2.32%)	2.16 (0.09)
	200.0	1.37×10 ⁻³⁴ (4.3%)	1.38×10 ⁻³⁴ (1.30%)	1.00 (0.04)	2.37×10 ⁻³⁴ (3.09%)	1.73 (0.09)	3.40×10 ⁻³⁴ (4.01%)	2.48 (0.15)
¹¹ C	10.5	1.77×10 ⁻³² (0.9%)	2.19×10 ⁻³² (0.63%)	1.24 (0.01)	2.71×10 ⁻³² (0.15%)	1.53 (0.01)	3.90×10 ⁻³² (0.18%)	2.20 (0.02)
	85.4	1.68×10 ⁻³³ (3.2%)	2.49×10 ⁻³³ (0.57%)	1.48 (0.05)	3.16×10 ⁻³³ (0.43%)	1.88 (0.06)	4.34×10 ⁻³³ (0.52%)	2.59 (0.08)
	160.4	2.67×10 ⁻³⁴ (4.9%)	3.59×10 ⁻³⁴ (0.75%)	1.35 (0.07)	4.81×10 ⁻³⁴ (1.11%)	1.80 (0.09)	6.89×10 ⁻³⁴ (1.35%)	2.58 (0.13)
	200.0	1.06×10 ⁻³⁴ (12.7%)	1.43×10 ⁻³⁴ (0.84%)	1.35 (0.17)	2.04×10 ⁻³⁴ (1.74%)	1.92 (0.25)	2.79×10 ⁻³⁴ (2.13%)	2.63 (0.34)
²⁰⁶ Bi	10.5	1.76×10 ⁻³¹ (1.4%)	2.17×10 ⁻³¹ (0.99%)	1.23 (0.02)	2.79×10 ⁻³¹ (0.29%)	1.58 (0.02)	4.25×10 ⁻³¹ (0.33%)	2.41 (0.04)
	85.4	1.91×10 ⁻³² (1.9%)	1.99×10 ⁻³² (0.92%)	1.04 (0.02)	2.62×10 ⁻³² (0.90%)	1.37 (0.03)	3.91×10 ⁻³² (1.06%)	2.05 (0.04)
	160.4	2.39×10 ⁻³³ (2.7%)	2.81×10 ⁻³³ (1.35%)	1.17 (0.04)	3.99×10 ⁻³³ (2.32%)	1.67 (0.06)	6.31×10 ⁻³³ (2.69%)	2.64 (0.10)
	200.0	1.10×10 ⁻³³ (1.9%)	1.11×10 ⁻³³ (1.53%)	1.01 (0.02)	1.71×10 ⁻³³ (3.80%)	1.56 (0.07)	2.39×10 ⁻³³ (4.63%)	2.18 (0.11)
²⁰⁵ Bi	10.5	1.83×10 ⁻³¹ (2.9%)	1.99×10 ⁻³¹ (0.92%)	1.09 (0.03)	2.35×10 ⁻³¹ (0.26%)	1.29 (0.04)	3.80×10 ⁻³¹ (0.30%)	2.08 (0.06)
	85.4	1.82×10 ⁻³² (3.7%)	1.95×10 ⁻³² (0.84%)	1.07 (0.04)	2.35×10 ⁻³² (0.80%)	1.29 (0.05)	3.63×10 ⁻³² (0.92%)	1.99 (0.08)
	160.4	2.59×10 ⁻³³ (5.2%)	2.73×10 ⁻³³ (1.28%)	1.05 (0.06)	3.55×10 ⁻³³ (2.14%)	1.37 (0.08)	5.76×10 ⁻³³ (2.35%)	2.22 (0.13)
	200.0	1.01×10 ⁻³³ (3.8%)	1.07×10 ⁻³³ (1.34%)	1.06 (0.04)	1.49×10 ⁻³³ (3.39%)	1.48 (0.08)	2.88×10 ⁻³³ (3.81%)	2.26 (0.12)
²⁰⁴ Bi	10.5	9.78×10 ⁻³² (1.9%)	1.39×10 ⁻³¹ (0.84%)	1.43 (0.03)	1.58×10 ⁻³¹ (0.23%)	1.62 (0.03)	2.55×10 ⁻³¹ (0.26%)	2.61 (0.05)
	85.4	1.40×10 ⁻³² (1.7%)	1.46×10 ⁻³² (0.73%)	1.04 (0.02)	1.72×10 ⁻³² (0.66%)	1.23 (0.02)	2.63×10 ⁻³² (0.77%)	1.88 (0.03)
	160.4	1.51×10 ⁻³³ (2.7%)	2.04×10 ⁻³³ (1.05%)	1.35 (0.04)	2.57×10 ⁻³³ (1.77%)	1.70 (0.05)	4.17×10 ⁻³³ (2.04%)	2.76 (0.09)
	200.0	7.77×10 ⁻³⁴ (1.7%)	8.12×10 ⁻³⁴ (1.20%)	1.05 (0.02)	1.08×10 ⁻³³ (2.77%)	1.38 (0.05)	1.65×10 ⁻³³ (3.14%)	2.12 (0.08)
²⁰³ Bi	10.5	1.00×10 ⁻³¹ (5.3%)	1.13×10 ⁻³¹ (0.87%)	1.13 (0.06)	1.27×10 ⁻³¹ (0.22%)	1.27 (0.07)	1.97×10 ⁻³¹ (0.26%)	1.97 (0.10)
	85.4	1.22×10 ⁻³² (4.9%)	1.27×10 ⁻³² (0.71%)	1.04 (0.05)	1.48×10 ⁻³² (0.62%)	1.21 (0.06)	2.21×10 ⁻³² (0.73%)	1.81 (0.09)
	160.4	1.57×10 ⁻³³ (6.8%)	1.78×10 ⁻³³ (0.99%)	1.13 (0.08)	2.19×10 ⁻³³ (1.59%)	1.40 (0.10)	3.52×10 ⁻³³ (1.91%)	2.24 (0.16)
	200.0	7.39×10 ⁻³⁴ (4.6%)	6.96×10 ⁻³⁴ (1.11%)	0.94 (0.04)	9.42×10 ⁻³⁴ (2.55%)	1.27 (0.07)	1.38×10 ⁻³³ (2.93%)	1.87 (0.10)
²⁰² Bi	10.5	6.87×10 ⁻³² (3.9%)	7.67×10 ⁻³² (0.95%)	1.12 (0.04)	8.54×10 ⁻³² (0.23%)	1.24 (0.05)	1.27×10 ⁻³¹ (0.27%)	1.85 (0.07)
	85.4	1.21×10 ⁻³² (5.8%)	9.10×10 ⁻³³ (0.74%)	0.75 (0.04)	1.05×10 ⁻³² (0.63%)	0.87 (0.05)	1.52×10 ⁻³² (0.75%)	1.26 (0.07)
	160.4	1.18×10 ⁻³³ (9.0%)	1.28×10 ⁻³³ (1.03%)	1.08 (0.10)	1.57×10 ⁻³³ (1.61%)	1.33 (0.12)	2.40×10 ⁻³³ (1.95%)	2.04 (0.19)
	200.0	5.91×10 ⁻³⁴ (7.7%)	4.97×10 ⁻³⁴ (1.14%)	0.84 (0.07)	6.79×10 ⁻³⁴ (2.51%)	1.15 (0.09)	9.59×10 ⁻³⁴ (3.02%)	1.62 (0.13)
²⁰¹ Bi	10.5	5.45×10 ⁻³² (11.8%)	5.46×10 ⁻³² (0.99%)	1.00 (0.12)	6.17×10 ⁻³² (0.22%)	1.13 (0.13)	8.62×10 ⁻³² (0.27%)	1.58 (0.19)
	85.4	5.00×10 ⁻³³ (31.2%)	6.86×10 ⁻³³ (0.76%)	1.37 (0.43)	8.04×10 ⁻³³ (0.59%)	1.61 (0.50)	1.10×10 ⁻³² (0.73%)	2.21 (0.69)
	160.4	1.09×10 ⁻³³ (24.7%)	9.75×10 ⁻³⁴ (1.01%)	0.89 (0.22)	1.23×10 ⁻³³ (1.52%)	1.12 (0.28)	1.74×10 ⁻³³ (1.87%)	1.60 (0.40)
	200.0	2.30×10 ⁻³⁴ (43.5%)	3.83×10 ⁻³⁴ (1.11%)	1.66 (0.72)	5.12×10 ⁻³⁴ (2.35%)	2.23 (0.97)	7.03×10 ⁻³⁴ (2.90%)	3.05 (1.33)
Average	10.5			1.12 (.008)		1.43 (.009)		2.09 (.013)
	85.4			1.02 (.009)		1.35 (.011)		2.01 (.017)
	160.4			1.14 (.017)		1.57 (.026)		2.41 (.042)
	200.0			1.00 (.013)		1.43 (.025)		2.11 (.041)

*: Relative error in %, **: Absolute error.

For steel shield, the attenuation length was obtained in this work at the material test location that comparatively agreed with the experimental data by Lee et al. [39]. The attenuation lengths for iron shield are also listed as reference, and those by Stevenson et al. [3] and by Nakashima et al. [8] agree well each other; however, attenuation length by Ban et al. [4] is much longer.

Generally, attenuation lengths evaluated by various experiments disperse, and this indicates the experimental attenuation lengths strongly depend on the surrounding shield structure. It can be said that a thick bulk shield with a wide plane and a simple structure with as little gap as possible is preferable to

obtain a practical attenuation length. However, each experimental data can be useful for benchmarking shielding simulations and for validating nuclear data and parameter used in the calculations.

4.2. Comparisons between experiment and simulation

Energy spectra in the energy range above 0.5 MeV were compared among the results by three simulation codes as shown in Figure 16 for the removable block, concrete, and steel shields, respectively. Generally, spectral shapes by the three codes are very similar

Table 5. Measured and simulated radionuclide production rates and C/Es in the concrete shield at the material test location.

	Thickness [cm]	Experiment [1/atom/p] (Err%*)	FLUKA		PHITS		GEANT4	
			[1/atom/p] (Err%*)	C/E (AbsErr**)	[1/atom/p] (Err%*)	C/E (AbsErr**)	[1/atom/p] (Err%*)	C/E (AbsErr**)
^{115m} In	0	1.80×10 ⁻³² (6.7%)	1.80×10 ⁻³² (1.08%)	1.00 (0.07)	2.28×10 ⁻³² (0.39%)	1.27 (0.08)	3.39×10 ⁻³² (0.48%)	1.88 (0.13)
	40	8.34×10 ⁻³³ (4.1%)	5.67×10 ⁻³³ (0.33%)	0.68 (0.03)	7.18×10 ⁻³³ (1.19%)	0.86 (0.04)	1.04×10 ⁻³² (1.31%)	1.24 (0.05)
	80	2.62×10 ⁻³³ (2.8%)	2.26×10 ⁻³³ (0.30%)	0.86 (0.02)	2.92×10 ⁻³³ (1.73%)	1.11 (0.04)	4.10×10 ⁻³³ (2.00%)	1.57 (0.05)
	120	1.21×10 ⁻³³ (5.4%)	9.17×10 ⁻³⁴ (0.32%)	0.76 (0.04)	1.09×10 ⁻³³ (2.39%)	0.90 (0.05)	1.67×10 ⁻³³ (2.91%)	1.38 (0.08)
	160	3.69×10 ⁻³⁴ (8.2%)	3.17×10 ⁻³⁴ (0.36%)	0.86 (0.07)	3.94×10 ⁻³⁴ (3.31%)	1.07 (0.09)	6.32×10 ⁻³⁴ (3.91%)	1.71 (0.16)
²⁴ Na	0	2.20×10 ⁻³³ (1.9%)	1.74×10 ⁻³³ (1.90%)	0.79 (0.02)	2.23×10 ⁻³³ (0.56%)	1.01 (0.02)	2.84×10 ⁻³³ (0.73%)	1.29 (0.03)
	40	1.02×10 ⁻³³ (4.2%)	7.94×10 ⁻³⁴ (0.60%)	0.78 (0.03)	1.00×10 ⁻³³ (1.40%)	0.98 (0.04)	1.29×10 ⁻³³ (1.58%)	1.26 (0.06)
	80	3.89×10 ⁻³⁴ (1.0%)	2.92×10 ⁻³⁴ (0.45%)	0.75 (0.01)	3.81×10 ⁻³⁴ (2.07%)	0.98 (0.02)	4.80×10 ⁻³⁴ (2.44%)	1.23 (0.03)
	120	1.29×10 ⁻³⁴ (3.9%)	1.09×10 ⁻³⁴ (0.42%)	0.84 (0.03)	1.29×10 ⁻³⁴ (3.14%)	1.00 (0.05)	1.80×10 ⁻³⁴ (3.36%)	1.40 (0.07)
	160	3.97×10 ⁻³⁵ (9.3%)	3.65×10 ⁻³⁵ (0.47%)	0.92 (0.09)	4.56×10 ⁻³⁵ (4.01%)	1.15 (0.12)	7.46×10 ⁻³⁵ (5.69%)	1.88 (0.21)
¹¹ C	0	2.12×10 ⁻³³ (1.3%)	2.06×10 ⁻³³ (1.86%)	0.97 (0.02)	2.48×10 ⁻³³ (0.30%)	1.17 (0.02)	2.98×10 ⁻³³ (0.40%)	1.40 (0.02)
	40	8.25×10 ⁻³⁴ (3.9%)	9.90×10 ⁻³⁴ (1.07%)	1.20 (0.05)	1.15×10 ⁻³³ (0.78%)	1.40 (0.06)	1.40×10 ⁻³³ (0.86%)	1.70 (0.07)
	80	3.21×10 ⁻³⁴ (5.9%)	3.62×10 ⁻³⁴ (0.78%)	1.13 (0.07)	4.28×10 ⁻³⁴ (1.15%)	1.33 (0.08)	5.32×10 ⁻³⁴ (1.33%)	1.66 (0.10)
	120	8.63×10 ⁻³⁵ (9.0%)	1.31×10 ⁻³⁴ (0.62%)	1.52 (0.14)	1.45×10 ⁻³⁴ (1.71%)	1.68 (0.15)	1.98×10 ⁻³⁴ (2.02%)	2.30 (0.21)
	160	3.38×10 ⁻³⁵ (9.5%)	4.40×10 ⁻³⁵ (0.55%)	1.30 (0.12)	5.04×10 ⁻³⁵ (2.30%)	1.49 (0.15)	6.96×10 ⁻³⁵ (2.86%)	2.06 (0.20)
²⁰⁶ Bi	0	1.46×10 ⁻³² (2.1%)	1.26×10 ⁻³² (2.74%)	0.86 (0.03)	1.47×10 ⁻³² (0.68%)	1.01 (0.02)	2.04×10 ⁻³² (0.83%)	1.39 (0.03)
	40	1.02×10 ⁻³² (4.1%)	6.41×10 ⁻³³ (0.52%)	0.63 (0.03)	7.67×10 ⁻³³ (1.75%)	0.75 (0.03)	9.95×10 ⁻³³ (1.83%)	0.98 (0.04)
	80	3.08×10 ⁻³³ (1.7%)	2.29×10 ⁻³³ (0.42%)	0.74 (0.01)	2.86×10 ⁻³³ (2.66%)	0.93 (0.03)	3.65×10 ⁻³³ (3.04%)	1.19 (0.04)
	120	1.20×10 ⁻³³ (6.1%)	8.22×10 ⁻³⁴ (0.48%)	0.69 (0.04)	9.20×10 ⁻³⁴ (3.95%)	0.77 (0.06)	1.43×10 ⁻³³ (4.39%)	1.19 (0.09)
	160	3.48×10 ⁻³⁴ (5.4%)	2.76×10 ⁻³⁴ (0.50%)	0.79 (0.04)	3.05×10 ⁻³⁴ (4.93%)	0.88 (0.06)	4.92×10 ⁻³⁴ (6.06%)	1.41 (0.11)
²⁰⁵ Bi	0	1.67×10 ⁻³² (3.1%)	1.32×10 ⁻³² (2.79%)	0.79 (0.03)	1.39×10 ⁻³² (0.59%)	0.83 (0.03)	1.99×10 ⁻³² (0.72%)	1.19 (0.04)
	40	9.29×10 ⁻³³ (9.4%)	6.48×10 ⁻³³ (0.58%)	0.70 (0.07)	7.17×10 ⁻³³ (1.54%)	0.77 (0.07)	9.63×10 ⁻³³ (1.57%)	1.04 (0.10)
	80	2.80×10 ⁻³³ (4.0%)	2.30×10 ⁻³³ (0.40%)	0.82 (0.03)	2.54×10 ⁻³³ (2.30%)	0.91 (0.04)	3.54×10 ⁻³³ (2.58%)	1.26 (0.06)
	120	9.15×10 ⁻³⁴ (12.2%)	8.23×10 ⁻³⁴ (0.42%)	0.90 (0.11)	8.35×10 ⁻³⁴ (3.63%)	0.91 (0.12)	1.30×10 ⁻³³ (3.95%)	1.43 (0.18)
	160	4.81×10 ⁻³⁴ (9.2%)	2.77×10 ⁻³⁴ (0.49%)	0.58 (0.05)	3.09×10 ⁻³⁴ (4.73%)	0.64 (0.07)	4.96×10 ⁻³⁴ (5.61%)	1.03 (0.11)
²⁰⁴ Bi	0	9.58×10 ⁻³³ (1.2%)	1.02×10 ⁻³² (2.36%)	1.07 (0.03)	1.12×10 ⁻³² (0.48%)	1.17 (0.01)	1.54×10 ⁻³² (0.60%)	1.61 (0.02)
	40	6.77×10 ⁻³³ (2.0%)	5.16×10 ⁻³³ (0.72%)	0.76 (0.02)	5.51×10 ⁻³³ (1.24%)	0.81 (0.02)	7.67×10 ⁻³³ (1.30%)	1.13 (0.03)
	80	1.99×10 ⁻³³ (1.2%)	1.85×10 ⁻³³ (0.44%)	0.93 (0.01)	1.98×10 ⁻³³ (1.83%)	0.99 (0.02)	2.75×10 ⁻³³ (2.04%)	1.38 (0.03)
	120	8.14×10 ⁻³⁴ (3.6%)	6.56×10 ⁻³⁴ (0.39%)	0.81 (0.03)	6.42×10 ⁻³⁴ (2.73%)	0.79 (0.04)	9.99×10 ⁻³⁴ (3.29%)	1.23 (0.06)
	160	2.21×10 ⁻³⁴ (4.0%)	2.20×10 ⁻³⁴ (0.48%)	1.00 (0.04)	2.28×10 ⁻³⁴ (3.82%)	1.03 (0.06)	3.70×10 ⁻³⁴ (4.46%)	1.67 (0.10)
²⁰³ Bi	0	1.12×10 ⁻³² (2.8%)	9.38×10 ⁻³³ (2.35%)	0.84 (0.03)	1.07×10 ⁻³² (0.43%)	0.95 (0.03)	1.39×10 ⁻³² (0.55%)	1.24 (0.04)
	40	5.91×10 ⁻³³ (5.9%)	4.71×10 ⁻³³ (0.91%)	0.80 (0.05)	5.02×10 ⁻³³ (1.12%)	0.85 (0.05)	6.90×10 ⁻³³ (1.20%)	1.17 (0.07)
	80	1.83×10 ⁻³³ (3.5%)	1.71×10 ⁻³³ (0.53%)	0.93 (0.03)	1.84×10 ⁻³³ (1.67%)	1.01 (0.04)	2.49×10 ⁻³³ (1.88%)	1.36 (0.05)
	120	7.39×10 ⁻³⁴ (10.7%)	6.04×10 ⁻³⁴ (0.43%)	0.82 (0.09)	6.01×10 ⁻³⁴ (2.52%)	0.81 (0.09)	9.20×10 ⁻³⁴ (2.89%)	1.24 (0.14)
	160	1.95×10 ⁻³⁴ (12.8%)	2.00×10 ⁻³⁴ (0.45%)	1.03 (0.13)	2.07×10 ⁻³⁴ (3.44%)	1.06 (0.14)	3.14×10 ⁻³⁴ (4.35%)	1.61 (0.22)
²⁰² Bi	0	9.74×10 ⁻³³ (3.4%)	7.12×10 ⁻³³ (2.48%)	0.73 (0.03)	8.12×10 ⁻³³ (0.44%)	0.83 (0.03)	1.02×10 ⁻³² (0.56%)	1.04 (0.04)
	40	5.51×10 ⁻³³ (3.5%)	3.51×10 ⁻³³ (1.09%)	0.64 (0.02)	3.72×10 ⁻³³ (1.13%)	0.67 (0.02)	4.94×10 ⁻³³ (1.22%)	0.90 (0.03)
	80	1.76×10 ⁻³³ (3.0%)	1.29×10 ⁻³³ (0.63%)	0.73 (0.02)	1.39×10 ⁻³³ (1.66%)	0.79 (0.03)	1.82×10 ⁻³³ (1.86%)	1.03 (0.04)
	120	7.11×10 ⁻³⁴ (6.2%)	4.56×10 ⁻³⁴ (0.48%)	0.64 (0.04)	4.57×10 ⁻³⁴ (2.50%)	0.64 (0.04)	6.79×10 ⁻³⁴ (2.83%)	0.95 (0.07)
	160	1.68×10 ⁻³⁴ (10.6%)	1.50×10 ⁻³⁴ (0.47%)	0.89 (0.09)	1.59×10 ⁻³⁴ (3.36%)	0.95 (0.11)	2.27×10 ⁻³⁴ (4.05%)	1.35 (0.15)
²⁰¹ Bi	0	5.59×10 ⁻³³ (12.6%)	5.86×10 ⁻³³ (2.48%)	1.05 (0.13)	6.74×10 ⁻³³ (0.41%)	1.21 (0.15)	8.07×10 ⁻³³ (0.54%)	1.44 (0.18)
	40	2.46×10 ⁻³³ (16.1%)	2.79×10 ⁻³³ (1.27%)	1.14 (0.18)	3.02×10 ⁻³³ (1.06%)	1.23 (0.20)	3.81×10 ⁻³³ (1.17%)	1.55 (0.25)
	80	9.94×10 ⁻³⁴ (10.4%)	1.04×10 ⁻³³ (0.78%)	1.05 (0.11)	1.13×10 ⁻³³ (1.54%)	1.14 (0.12)	1.47×10 ⁻³³ (1.77%)	1.47 (0.16)
	120	4.34×10 ⁻³⁴ (22.2%)	3.72×10 ⁻³⁴ (0.58%)	0.86 (0.19)	3.83×10 ⁻³⁴ (2.29%)	0.88 (0.20)	5.42×10 ⁻³⁴ (2.69%)	1.25 (0.28)
	160	1.80×10 ⁻³⁴ (21.7%)	1.22×10 ⁻³⁴ (0.52%)	0.68 (0.15)	1.34×10 ⁻³⁴ (3.03%)	0.74 (0.16)	1.80×10 ⁻³⁴ (3.77%)	1.00 (0.22)
Average	0			0.87 (.010)		1.06 (.008)		1.38 (.010)
	40			0.73 (.010)		0.82 (.012)		1.11 (.016)
	80			0.80 (.006)		0.96 (.011)		1.27 (.015)
	120			0.78 (.015)		0.82 (.019)		1.24 (.030)
	160			0.86 (.022)		0.94 (.029)		1.47 (.048)

*: Relative error in %, **: Absolute error.

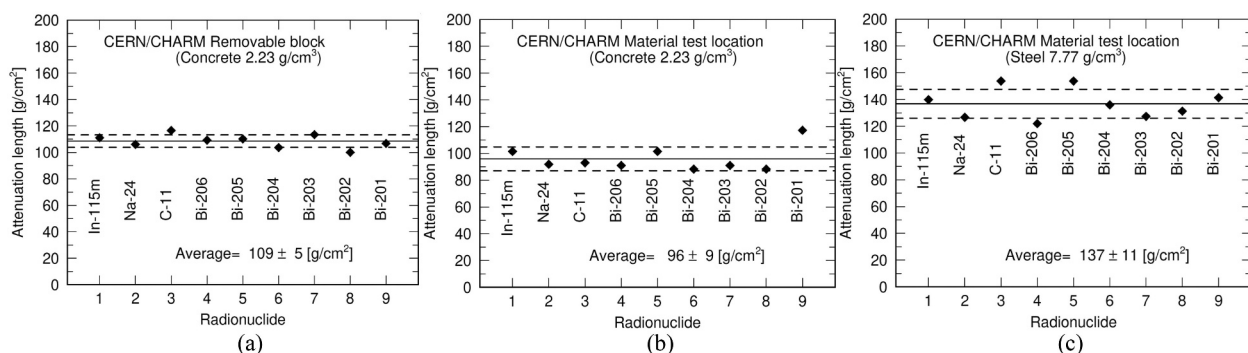
Table 6. Measured and simulated radionuclide production rates and C/E's in the steel shield at the material test location.

	Thickness [cm]	Experiment [1/atom/p] (Err%*)	FLUKA		PHITS		GEANT4	
			[1/atom/p] (Err%*)	C/E (AbsErr**)	[1/atom/p] (Err%*)	C/E (AbsErr**)	[1/atom/p] (Err%*)	C/E (AbsErr**)
^{115m} In	0	3.92×10 ⁻³² (3.1%)	3.19×10 ⁻³² (0.60%)	0.81 (0.03)	3.47×10 ⁻³² (0.37%)	0.89 (0.03)	5.44×10 ⁻³² (0.42%)	1.39 (0.04)
	20	2.12×10 ⁻³² (0.8%)	1.48×10 ⁻³² (0.20%)	0.70 (0.01)	1.61×10 ⁻³² (0.89%)	0.76 (0.01)	2.44×10 ⁻³² (0.86%)	1.15 (0.01)
	40	6.94×10 ⁻³³ (1.3%)	5.84×10 ⁻³³ (0.23%)	0.84 (0.01)	6.25×10 ⁻³³ (1.22%)	0.90 (0.02)	9.72×10 ⁻³³ (1.27%)	1.40 (0.03)
	60	2.55×10 ⁻³³ (4.0%)	2.08×10 ⁻³³ (0.32%)	0.82 (0.03)	2.14×10 ⁻³³ (1.84%)	0.84 (0.04)	3.32×10 ⁻³³ (1.89%)	1.30 (0.06)
	80	6.32×10 ⁻³⁴ (7.7%)	6.84×10 ⁻³⁴ (0.44%)	1.08 (0.08)	7.16×10 ⁻³⁴ (2.64%)	1.13 (0.09)	1.06×10 ⁻³³ (3.11%)	1.68 (0.14)
²⁴ Na	0	2.58×10 ⁻³³ (4.0%)	2.12×10 ⁻³³ (1.49%)	0.82 (0.03)	2.40×10 ⁻³³ (0.62%)	0.93 (0.04)	3.22×10 ⁻³³ (0.80%)	1.25 (0.05)
	20	1.17×10 ⁻³³ (1.4%)	1.04×10 ⁻³³ (0.49%)	0.89 (0.01)	1.26×10 ⁻³³ (1.45%)	1.08 (0.02)	1.66×10 ⁻³³ (1.58%)	1.42 (0.03)
	40	3.87×10 ⁻³⁴ (3.6%)	3.72×10 ⁻³⁴ (0.47%)	0.96 (0.04)	4.70×10 ⁻³⁴ (2.12%)	1.22 (0.05)	5.68×10 ⁻³⁴ (2.46%)	1.47 (0.06)
	60	1.03×10 ⁻³⁴ (5.0%)	1.25×10 ⁻³⁴ (0.63%)	1.22 (0.06)	1.55×10 ⁻³⁴ (3.41%)	1.50 (0.09)	1.87×10 ⁻³⁴ (4.29%)	1.82 (0.12)
	80	2.42×10 ⁻³⁵ (14.6%)	3.94×10 ⁻³⁵ (0.93%)	1.63 (0.24)	4.61×10 ⁻³⁵ (4.80%)	1.91 (0.29)	5.13×10 ⁻³⁵ (6.16%)	2.12 (0.34)
¹¹ C	0	1.89×10 ⁻³³ (3.0%)	2.21×10 ⁻³³ (1.78%)	1.17 (0.04)	2.51×10 ⁻³³ (0.33%)	1.33 (0.04)	3.03×10 ⁻³³ (0.42%)	1.60 (0.05)
	20	7.83×10 ⁻³⁴ (2.0%)	9.76×10 ⁻³⁴ (0.95%)	1.25 (0.03)	1.15×10 ⁻³³ (0.85%)	1.47 (0.03)	1.46×10 ⁻³³ (0.92%)	1.87 (0.04)
	40	2.30×10 ⁻³⁴ (4.0%)	3.37×10 ⁻³⁴ (0.63%)	1.46 (0.06)	4.02×10 ⁻³⁴ (1.26%)	1.75 (0.07)	4.93×10 ⁻³⁴ (1.46%)	2.14 (0.09)
	60	9.17×10 ⁻³⁵ (10.2%)	1.12×10 ⁻³⁴ (0.53%)	1.22 (0.12)	1.30×10 ⁻³⁴ (2.00%)	1.41 (0.15)	1.56×10 ⁻³⁴ (2.41%)	1.70 (0.18)
	80	3.12×10 ⁻³⁵ (10.1%)	3.53×10 ⁻³⁵ (0.64%)	1.13 (0.11)	4.09×10 ⁻³⁵ (2.84%)	1.31 (0.14)	4.68×10 ⁻³⁵ (3.84%)	1.50 (0.16)
²⁰⁶ Bi	0	2.28×10 ⁻³² (5.1%)	1.31×10 ⁻³² (2.50%)	0.57 (0.03)	1.56×10 ⁻³² (0.76%)	0.69 (0.04)	2.13×10 ⁻³² (0.89%)	0.94 (0.05)
	20	1.23×10 ⁻³² (1.8%)	7.34×10 ⁻³³ (0.60%)	0.60 (0.01)	9.29×10 ⁻³³ (1.83%)	0.76 (0.02)	1.32×10 ⁻³² (1.86%)	1.07 (0.03)
	40	4.21×10 ⁻³³ (2.9%)	2.57×10 ⁻³³ (0.56%)	0.61 (0.02)	3.26×10 ⁻³³ (2.67%)	0.77 (0.03)	4.34×10 ⁻³³ (2.90%)	1.03 (0.04)
	60	1.05×10 ⁻³³ (7.7%)	8.54×10 ⁻³⁴ (0.72%)	0.81 (0.06)	9.89×10 ⁻³⁴ (4.26%)	0.94 (0.08)	1.39×10 ⁻³³ (4.63%)	1.32 (0.12)
	80	2.15×10 ⁻³⁴ (9.8%)	2.67×10 ⁻³⁴ (1.06%)	1.24 (0.12)	3.36×10 ⁻³⁴ (5.78%)	1.56 (0.18)	4.15×10 ⁻³⁴ (7.18%)	1.93 (0.23)
²⁰⁵ Bi	0	3.10×10 ⁻³² (10.6%)	1.30×10 ⁻³² (2.45%)	0.42 (0.05)	1.44×10 ⁻³² (0.65%)	0.46 (0.05)	2.04×10 ⁻³² (0.80%)	0.66 (0.07)
	20	1.07×10 ⁻³² (3.6%)	6.96×10 ⁻³³ (0.65%)	0.65 (0.02)	8.09×10 ⁻³³ (1.67%)	0.76 (0.03)	1.15×10 ⁻³² (1.65%)	1.07 (0.04)
	40	3.41×10 ⁻³³ (7.4%)	2.43×10 ⁻³³ (0.52%)	0.71 (0.05)	2.83×10 ⁻³³ (2.38%)	0.83 (0.06)	3.96×10 ⁻³³ (2.57%)	1.16 (0.09)
	60	1.07×10 ⁻³³ (17.7%)	8.04×10 ⁻³⁴ (0.69%)	0.75 (0.13)	8.78×10 ⁻³⁴ (3.93%)	0.82 (0.15)	1.28×10 ⁻³³ (4.14%)	1.20 (0.22)
	80	4.32×10 ⁻³⁴ (13.9%)	2.54×10 ⁻³⁴ (1.09%)	0.59 (0.08)	2.94×10 ⁻³⁴ (5.59%)	0.68 (0.10)	4.01×10 ⁻³⁴ (6.64%)	0.93 (0.14)
²⁰⁴ Bi	0	1.52×10 ⁻³² (2.5%)	1.10×10 ⁻³² (2.29%)	0.72 (0.02)	1.15×10 ⁻³² (0.52%)	0.76 (0.02)	1.57×10 ⁻³² (0.64%)	1.03 (0.03)
	20	7.32×10 ⁻³³ (0.9%)	5.28×10 ⁻³³ (0.75%)	0.72 (0.01)	5.77×10 ⁻³³ (1.35%)	0.79 (0.01)	8.28×10 ⁻³³ (1.40%)	1.13 (0.02)
	40	2.39×10 ⁻³³ (1.6%)	1.83×10 ⁻³³ (0.49%)	0.77 (0.01)	2.04×10 ⁻³³ (2.02%)	0.85 (0.02)	2.76×10 ⁻³³ (2.17%)	1.15 (0.03)
	60	6.36×10 ⁻³⁴ (4.1%)	6.03×10 ⁻³⁴ (0.57%)	0.95 (0.04)	6.46×10 ⁻³⁴ (3.19%)	1.02 (0.05)	9.08×10 ⁻³⁴ (3.62%)	1.43 (0.08)
	80	1.92×10 ⁻³⁴ (5.8%)	1.90×10 ⁻³⁴ (0.89%)	0.99 (0.06)	2.03×10 ⁻³⁴ (4.70%)	1.06 (0.08)	2.83×10 ⁻³⁴ (5.92%)	1.48 (0.12)
²⁰³ Bi	0	1.40×10 ⁻³² (7.3%)	1.04×10 ⁻³² (2.29%)	0.74 (0.06)	1.08×10 ⁻³² (0.47%)	0.77 (0.06)	1.41×10 ⁻³² (0.60%)	1.00 (0.07)
	20	5.98×10 ⁻³³ (2.7%)	4.69×10 ⁻³³ (0.92%)	0.78 (0.02)	5.05×10 ⁻³³ (1.25%)	0.84 (0.03)	7.04×10 ⁻³³ (1.33%)	1.18 (0.04)
	40	1.93×10 ⁻³³ (4.8%)	1.60×10 ⁻³³ (0.54%)	0.83 (0.04)	1.75×10 ⁻³³ (1.85%)	0.91 (0.05)	2.37×10 ⁻³³ (2.10%)	1.23 (0.06)
	60	5.55×10 ⁻³⁴ (12.4%)	5.32×10 ⁻³⁴ (0.58%)	0.96 (0.12)	5.72×10 ⁻³⁴ (2.87%)	1.03 (0.13)	7.51×10 ⁻³⁴ (3.49%)	1.35 (0.17)
	80	1.27×10 ⁻³⁴ (21.3%)	1.66×10 ⁻³⁴ (0.85%)	1.31 (0.28)	1.78×10 ⁻³⁴ (4.18%)	1.40 (0.30)	2.22×10 ⁻³⁴ (5.39%)	1.75 (0.38)
²⁰² Bi	0	1.33×10 ⁻³² (4.8%)	7.89×10 ⁻³³ (2.42%)	0.59 (0.03)	8.10×10 ⁻³³ (0.48%)	0.61 (0.03)	1.03×10 ⁻³² (0.61%)	0.77 (0.04)
	20	5.33×10 ⁻³³ (2.1%)	3.43×10 ⁻³³ (1.08%)	0.64 (0.02)	3.64×10 ⁻³³ (1.27%)	0.68 (0.02)	4.90×10 ⁻³³ (1.35%)	0.92 (0.02)
	40	1.77×10 ⁻³³ (3.9%)	1.17×10 ⁻³³ (0.61%)	0.66 (0.03)	1.26×10 ⁻³³ (1.90%)	0.71 (0.03)	1.69×10 ⁻³³ (2.18%)	0.95 (0.04)
	60	4.33×10 ⁻³⁴ (9.6%)	3.88×10 ⁻³⁴ (0.60%)	0.90 (0.09)	4.18×10 ⁻³⁴ (2.96%)	0.96 (0.10)	5.06×10 ⁻³⁴ (3.66%)	1.17 (0.12)
	80	1.32×10 ⁻³⁴ (14.5%)	1.22×10 ⁻³⁴ (0.94%)	0.92 (0.13)	1.30×10 ⁻³⁴ (4.27%)	0.99 (0.15)	1.48×10 ⁻³⁴ (5.66%)	1.12 (0.18)
²⁰¹ Bi	0	6.28×10 ⁻³³ (17.7%)	6.38×10 ⁻³³ (2.38%)	1.02 (0.18)	6.68×10 ⁻³³ (0.45%)	1.06 (0.19)	8.10×10 ⁻³³ (0.57%)	1.29 (0.23)
	20	3.03×10 ⁻³³ (7.1%)	2.67×10 ⁻³³ (1.24%)	0.88 (0.06)	2.88×10 ⁻³³ (1.19%)	0.95 (0.07)	3.67×10 ⁻³³ (1.31%)	1.21 (0.09)
	40	8.77×10 ⁻³⁴ (14.6%)	9.19×10 ⁻³⁴ (0.71%)	1.05 (0.15)	1.03×10 ⁻³³ (1.77%)	1.17 (0.17)	1.25×10 ⁻³³ (2.10%)	1.43 (0.21)
	60	1.96×10 ⁻³⁴ (47.3%)	3.04×10 ⁻³⁴ (0.62%)	1.55 (0.73)	3.34×10 ⁻³⁴ (2.76%)	1.71 (0.81)	3.80×10 ⁻³⁴ (3.54%)	1.94 (0.92)
	80	9.61×10 ⁻³⁵ (45.6%)	9.59×10 ⁻³⁵ (0.88%)	1.00 (0.46)	1.03×10 ⁻³⁴ (3.91%)	1.07 (0.49)	1.10×10 ⁻³⁴ (5.55%)	1.15 (0.53)
Average	0			0.73 (.012)		0.80 (.011)		1.08 (.015)
	20			0.72 (.004)		0.81 (.006)		1.16 (.008)
	40			0.78 (.007)		0.88 (.010)		1.25 (.015)
	60			0.92 (.020)		0.97 (.025)		1.38 (.036)
	80			0.98 (.035)		1.08 (.043)		1.43 (.060)

*: Relative error in %, **: Absolute error.

Table 7. Summary of uncertainties.

	Source of uncertainty	Uncertainty on production rate
Experiment	γ -spectrometry statistics	1.78–9.58%
	γ -spectrometry efficiency	4.3%
	Activation detector weight	1%
	Beam monitor calibration	7%
	Beam intensity statistics	<1%
	Beam momentum	<1%
	Beam position and profile	<1%
	Target density and dimension	<1%
	Simulation	Statistics (FLUKA)
	Statistics (PHITS)	.14–5.78%
	Statistics (GEANT4)	.16–6.64%

**Figure 15.** Attenuation lengths estimated in (a) removable block, (b) concrete and (c) steel shields at material test location.**Table 8.** Summary of attenuation length (λ) for cited experiments at facilities with high-energy protons (>10 GeV) compared with this work.

Material	Author	Facility	Proton Energy	Detector	Density [g/cm ³]	λ [g/cm ²]		
Concrete	Stevenson et al. [3]	CERN-PS	25.5 GeV	C,Al	2.35	120		
	Ban et al. [4]	KEK-PS	12 GeV	C,Al		143		
	Nakashima et al. [8]	BNL-AGS	24 GeV	Bi	2.45	90.5		
	Nakao et al. [17]	CERN-CHARM Original bulk shield	24 GeV	Bi,Al	2.4	120	\pm	7
	This work	CERN-CHARM Removal sample block	24 GeV	Bi,Al,In,C	2.23	109	\pm	5
	This work	CERN-CHARM Material test location	24 GeV	Bi,Al,In,C	2.23	96	\pm	9
	Lee et al. [39]	CERN-CHARM Material test location	24 GeV	NE213	2.23*	98*	\pm	7
Iron	Stevenson et al. [3]	CERN-PS	25.5 GeV	C,Al	7.87	147		
	Ban et al. [4]	KEK-PS	12 GeV	C,Al	7.08	188	\pm	12
	Nakashima et al. [8]	BNL-AGS	24 GeV	Bi	7.74	149		
Steel	This work	CERN-CHARM Material test location	24 GeV	Bi,Al,In,C	7.77	137	\pm	11
	Lee et al. [39]	CERN-CHARM Material test location	24 GeV	NE213	7.77*	132*	\pm	4

*re-evaluated attenuation lengths with re-evaluated material densities.

and only absolute value differences can be found. The spectra by PHITS and GEANT4 gave within around 1.5- and 2-times higher value, respectively, than those by FLUKA. Since the attenuations through the shield thickness are almost same among the results by the three codes, these absolute value differences would be attributed from neutron production from the copper target at side direction. As shown in Figure 16 (b) and (c), neutron spectra at 0-cm thickness, which are equivalent to the source term at 90 degrees from the copper target, indicated discrepancy between the three

simulation codes. It is considered that this discrepancy was caused by the difference of nuclear models, their parameters, and the database for secondary particle productions from copper target. Therefore, in the future, it is expected that the differential particle production in this energy range will be experimentally evaluated and accuracies of database in the simulations will be improved.

Simulated radionuclide production rates were compared with the experimental data as shown in Figures 12, 13, and 14 for the removable block, concrete, and

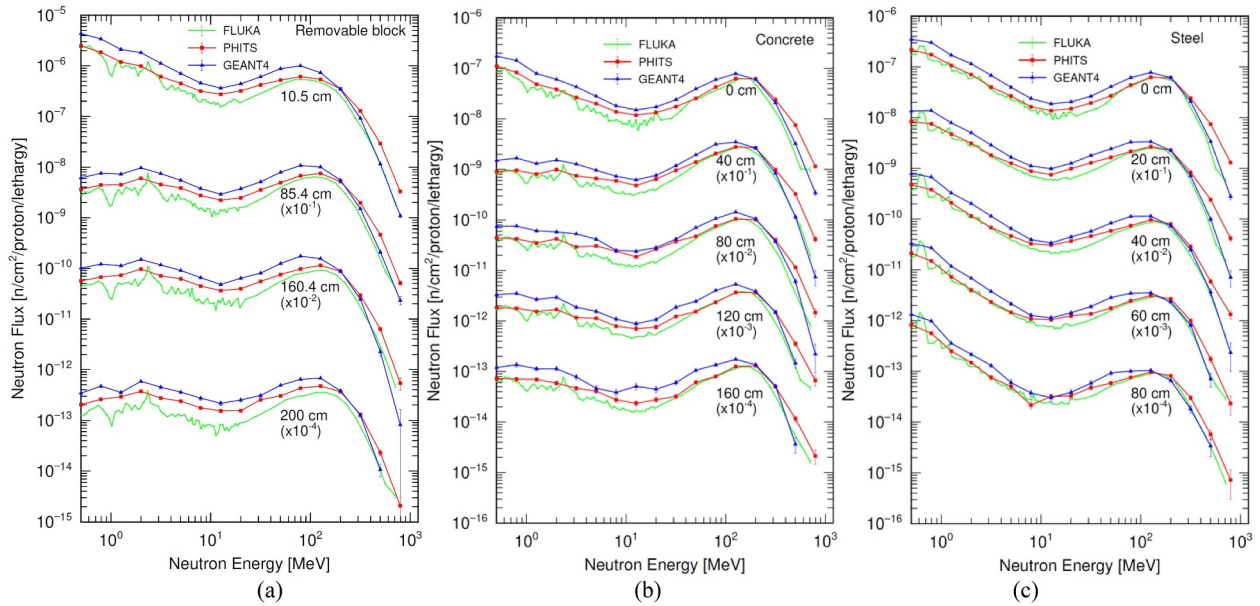


Figure 16. Simulated energy spectra of neutrons in (a) removable block, (b) concrete and (c) steel shields at material test location.

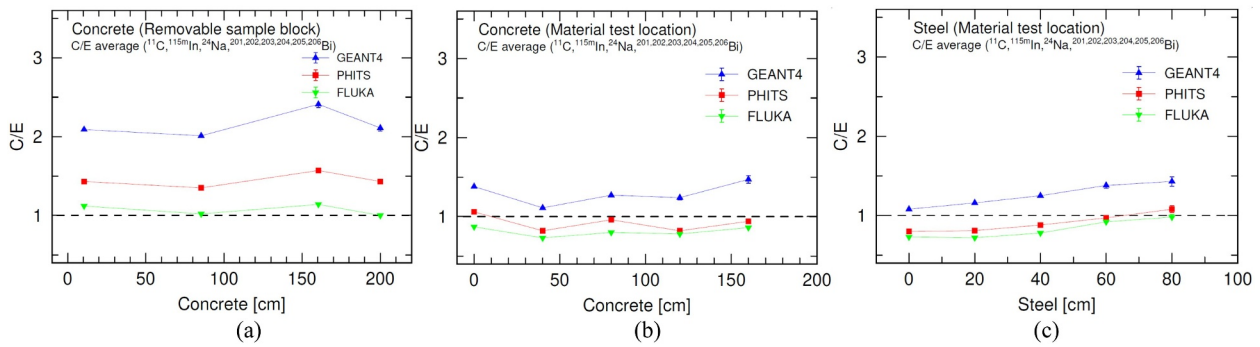


Figure 17. Average C/E ratios of production rates estimated in (a) removable block, (b) concrete and (c) steel shields at material test location.

steel shields, respectively. C/E , that is ratio of calculated to experimental results, was estimated for each production rate and listed in Tables 4, 5, and 6. To observe tendencies of C/E for all nuclides, average- C/E s were estimated by error-weighted averaging over the C/E s for all production rates as shown in Figure 17. From Figure 17(a) and Table 4 for removable block, average- C/E s of FLUKA ranged from 1.00 to 1.14, which showed very good agreement with the experiment. Those of PHITS and GEANT4 ranged from 1.35 to 1.57 and from 2.01 to 2.41, respectively, which showed overestimations by 35–57% for PHITS and by more than a factor of 2 for GEANT4. From Figure 17(b) and Table 5 for concrete shield, average C/E s ranged from 0.73 to 0.87 for FLUKA, 0.82 to 1.06 for PHITS, and 1.11 to 1.47 for GEANT4. From Figure 17(c) and Table 6 for steel shield, average- C/E s ranged from 0.72 to 0.98 for FLUKA, 0.80 to 1.08 for PHITS, and 1.08 to 1.43 for GEANT4. Maximum discrepancies from the experimental data were finally estimated to be 28% for FLUKA, 57% for PHITS, and 141% for GEANT4.

5. Conclusion

A high-energy neutron shielding experiment with various thickness of concrete and steel was performed using bismuth, indium, aluminum, and graphite activation detectors. Neutrons were generated by a 24-GeV/c proton beam injected into a 50-cm-thick copper target in the CHARM facility at CERN. The radionuclide production rates of the reactions of $^{209}\text{Bi}(n,xn)^{210-x}\text{Bi}(x=4-9)$, $^{115}\text{In}(n,n')^{115\text{m}}\text{In}$, $^{27}\text{Al}(n,\alpha)^{24}\text{Na}$, and $^{12}\text{C}(n,2n)^{11}\text{C}$ were measured at various concrete and steel thicknesses, and the attenuation profiles of concrete and steel shields were obtained, respectively. Attenuation lengths of neutrons for concrete and steel were evaluated from the experimental results. Two different set-ups of experiment with a removable block and a material test location were performed, and the attenuation lengths of concrete evaluated from those two set-ups showed discrepancy due to the surrounding shield structures. Furthermore, attenuation lengths of this work and the other

cited experimental data disperse, which indicates that the attenuation lengths strongly depend on the shield structure and measuring conditions. Shielding experiments with a simple structure and a wide plane of shields are needed to obtain accurate attenuation lengths. However, this work provides good benchmark data of a deep-shield penetration in a high-energy proton accelerator facility. The results are expected to improve our understanding of the shielding design in future high-energy accelerator facilities. Simulations with three Monte Carlo codes were also performed to compare with the experimental data, and maximum discrepancies from the experiment were obtained to be 28% for FLUKA, 57% for PHITS, and 141% for GEANT4, demonstrating their fit-for-purposeness for shielding design calculations.

Acknowledgments

The authors are deeply grateful to the accelerator operation staff and the experimental groups at the IRRAD and the CHARM for their helpful support in the experiment. They are also grateful to Nicolas Riggaz and the staff of the gamma-spectrometry lab at CERN for their support in measurement and analysis of the germanium detectors.

Disclosure statement

No potential conflict of interest was reported by the author(s).

ORCID

Noriaki Nakao  <http://orcid.org/0000-0002-5910-8222>
 Toshiya Sanami  <http://orcid.org/0000-0003-2255-8008>
 Tsuyoshi Kajimoto  <http://orcid.org/0009-0003-6133-3888>
 Hiroshi Yashima  <http://orcid.org/0000-0003-0931-5984>
 Robert Froeschl  <http://orcid.org/0000-0002-2194-5869>
 Davide Bozzato  <http://orcid.org/0000-0001-5306-361X>
 Elpida Iliopoulou  <http://orcid.org/0000-0003-0895-9227>
 Angelo Infantino  <http://orcid.org/0000-0002-7854-3502>
 Eunji Lee  <http://orcid.org/0000-0002-0600-2571>
 Takahiro Oyama  <http://orcid.org/0000-0002-9425-0275>
 Masayuki Hagiwara  <http://orcid.org/0000-0003-0236-2905>
 Tetsuro Matsumoto  <http://orcid.org/0000-0003-2047-7028>
 Akihiko Masuda  <http://orcid.org/0000-0003-0572-0341>
 Yoshitomo Uwamino  <http://orcid.org/0000-0002-8359-3520>
 Arnaud Devienne  <http://orcid.org/0009-0002-4837-3810>
 Fabio Pozzi  <http://orcid.org/0000-0002-3980-5303>
 Tommaso Lorenzon  <http://orcid.org/0009-0006-3898-0704>
 Nabil Mena  <http://orcid.org/0000-0002-8509-9665>
 Heinz Vincke  <http://orcid.org/0000-0003-3593-4818>
 Stefan Roesler  <http://orcid.org/0000-0002-5920-0459>
 Markus Brugger  <http://orcid.org/0000-0002-3645-7091>

References

- [1] Moyer BJP. 1st Int. Conf. Shielding around high energy accelerators. Presses Universitaires de France; Paris. 1962: p 65.
- [2] Tesch K. A simple estimation of the lateral shielding for proton accelerators in the energy range 50 to 1000 MeV. *Radiat Prot Dosimetry*. 1985;11(3):165–172. doi: 10.1093/oxfordjournals.rpd.a079462
- [3] Stevenson GR, Liu KL, Thomas RH. Determination of transverse shielding for proton accelerators using the Moyer model. *Health Phys*. 1982;43(1):13–29. doi: 10.1097/00004032-198207000-00002
- [4] Ban S, Hirayama H, Kondo K, et al. Measurement of transverse attenuation lengths for paraffin, heavy concrete and iron around an external target for 12 GeV protons. *Nucl Instr Meth*. 1980;174(1–2):271–276. doi: 10.1016/0029-554X(80)90441-3
- [5] Ban S, Hirayama H, Katoh K. Measurement of secondary neutron fluences around beam stop for 500 MeV protons. *Nucl Instr Meth*. 1981;184(2–3):409–412. doi: 10.1016/0029-554X(81)90739-4
- [6] Bull JS, Donahue JB, Burman RL. Measurement of neutron attenuation through thick shields and comparison with calculation. Proc. 4th Workshop on Simulating Accelerator Radiation Environments (SARE4), Knoxville, Tennessee, 1998 September 14–16:201–208.
- [7] Nunomiya T, Nakao N, Wright P et al. Measurement of deep penetration of neutrons produced by 800-MeV proton beam through concrete and iron at ISIS. *Nucl Instr Meth*. 2001;B179(1):89–102. doi: 10.1016/S0168-583X(01)00387-1
- [8] Nakashima H, Takada H, Kasugai Y et al. Research activities on Neutronics under ASTE collaboration at AGS/BNL. *Nucl Sci Technol*. 2002;2:1155–1160. doi: 10.1080/00223131.2002.10875307
- [9] Nakashima H, Mokhov NV, Kasugai Y et al. Research activities on JASMIN: Japanese and American study of muon interaction and neutron detection. Proc. 12th International Conference on Radiation Shielding (ICRS-12) and the 17th Topical Meeting of the Radiation Protection and Shielding Division of ANS (RPSD-2012); 2–7 September 2012, Nara, Japan, Nuclear Science and Technology; 2014;4:191–196.
- [10] Nakao N, Nakashima H, Nakamura T et al. Transmission through shields of quasi-monoenergetic neutrons generated by 43- and 68-MeV protons —I: concrete shielding experiment and calculation for practical application. *Nucl Sci Eng*. 1996;124(2):228–242. doi: 10.13182/NSE96-A28574
- [11] Nakashima H, Nakao N, Tanaka S et al. Transmission through shields of quasi-monoenergetic neutrons generated by 43- and 68-MeV protons —II: iron shielding experiment and analysis for investigating calculational method and cross-section data. *Nucl Sci Eng*. 1996;124(2):243–257. doi: 10.13182/NSE96-A28575
- [12] Nakao N, Nakao M, Nakashima H, et al. Measurements and calculations of neutron energy spectra behind polyethylene shields bombarded by 40- and 65-MeV quasi-monoenergetic neutron sources. *J Nucl Sci Technol*. 1997;34(4):348–359. doi: 10.1080/18811248.1997.9733674
- [13] Nakao N, Yashima H, Kawai M et al. Arrangement of high-energy neutron irradiation field and shielding

- experiment using 4 m concrete at KENS. Proc 10th International Conference On Radiation Shielding (ICRS10), Madeira, Portugal, 2004 May 9–14: Radiat Prot Dosim. 2005;116(1–4):553–557.
- [14] Nakao N, Taniguchi S, Roesler S et al. Measurement and calculation of high-energy neutron spectra behind shielding at the CERF 120 GeV/c hadron beam facility. Nucl Instr Meth. 2008;B266(1):93–106. doi: [10.1016/j.nimb.2007.09.043](https://doi.org/10.1016/j.nimb.2007.09.043)
- [15] Froeschl R Radiation protection assessment of the proton irradiation facility and the CHARM facility in the east area, Tech. Rep. CERN-RP-2014-008-REPORTS-TN, EDMS, 2014:1355933.
- [16] Froeschl R, Brugger M, Roesler S. The CERN high energy accelerator mixed field (CHARM) facility in the CERN PS east experimental area. Proc of SATIF-12 Batavia, Illinois, United States, 2014 Apr NEA/NSC/R. 2015;3:14–25.
- [17] Nakao N, Sanami T, Kajimoto T, et al. Attenuation length of high energy neutrons through a thick concrete shield measured by activation detectors at CHARM. J Nucl Sci Technol. 2020;57(9):1022–1034. doi: [10.1080/00223131.2020.1751740](https://doi.org/10.1080/00223131.2020.1751740)
- [18] Iliopoulou E, Bamidis P, Brugger M et al. Measurements and FLUKA simulations of bismuth and aluminium activation at the CERN shielding benchmark facility (CSBF). Nucl Instr Meth. 2018; A855:79–85. doi: [10.1016/j.nima.2017.12.058](https://doi.org/10.1016/j.nima.2017.12.058)
- [19] Kajimoto T, Sanami T, Nakao N et al. Neutron energy spectrum measurement using an NE213 scintillator at CHARM. Nucl Instr Meth. 2018;B429:27–33. doi: [10.1016/j.nimb.2018.05.024](https://doi.org/10.1016/j.nimb.2018.05.024)
- [20] Kajimoto T, Sanami T, Nakao N et al. Reproduction of neutron fluence by unfolding method with an NE213 scintillator. Nucl Instr Meth. 2018;A906:141–149. doi: [10.1016/j.nima.2018.07.079](https://doi.org/10.1016/j.nima.2018.07.079)
- [21] Gkotse B, Glaser M, Lima P et al. A new high-intensity proton irradiation facility at the CERN PS east area. Proceedings of Science, Technology and Instrumentation in Particle Physics 2014, 2-6 June, 2014, Amsterdam, the Netherland. <https://pos.sissa.it/213/354/>
- [22] Nakao N, Uwamino Y, Tanaka K. Measurement of the neutron angular distribution from a beryllium target bombarded with a 345-MeV/u ²³⁸U beam at the RIKEN RI beam factory. Nucl Instr Meth. 2018; B423:27–36. doi: [10.1016/j.nimb.2018.02.036](https://doi.org/10.1016/j.nimb.2018.02.036)
- [23] Gatignon L. Beam properties for the east area irradiation facility in the T8 beam line. Tech Rep. EDMS, CERN. 2013;1270807.
- [24] Bernier K, de Rijk G, Ferioli G, et al. Calibration of secondary emission monitors of absolute proton beam intensity in the CERN SPS North area. CERN Yellow Report. 1997;97-07:22.
- [25] Glaser M, Ravotti F, Moll M, et al. Dosimetry assessments in the irradiation facilities at the CERN-PS accelerator. IEEE Trans Nucl Sci. 2006;53(4):2016–2022. doi: [10.1109/TNS.2006.880569](https://doi.org/10.1109/TNS.2006.880569)
- [26] Bronson FL. Validation of the accuracy of the LabSOCS software for mathematical efficiency calibration of Ge detectors for typical laboratory samples. J Radioanal Nucl Chem. 2003;255(1):137–141. doi: [10.1023/A:1022248318741](https://doi.org/10.1023/A:1022248318741)
- [27] Sato T, Iwamoto Y, Hashimoto S, et al. Features of particle and heavy ion transport code system PHITS version 3.02. J Nucl Sci Technol. 2018;55(6):684–690. doi: [10.1080/00223131.2017.1419890](https://doi.org/10.1080/00223131.2017.1419890)
- [28] Hirayama H, Namito Y, F BA et al. The EGS5 code system. SLAC-R-730. 2005, KEK Report 2005-8. 2005.
- [29] Ahdida C, Bozzato D, Calzolari D, et al. New capabilities of the FLUKA multi-purpose code. Front Phys. 2022;9:788253. doi: [10.3389/fphy.2021.788253](https://doi.org/10.3389/fphy.2021.788253)
- [30] Battistoni G, Boehlen T, Cerutti F, et al. Overview of the FLUKA code. Ann Nucl Energy. 2015;82:10–18. doi: [10.1016/j.anucene.2014.11.007](https://doi.org/10.1016/j.anucene.2014.11.007)
- [31] Allison J, Amako K, Apostolakis J, et al. Recent developments in GEANT4. Nucl Instr Meth. 2016; A835:186–225. doi: [10.1016/j.nima.2016.06.125](https://doi.org/10.1016/j.nima.2016.06.125)
- [32] Agostinelli S, Allison J, Amako K, et al. Geant4 – a simulation toolkit. Nucl Instr Meth. 2003;A506:250–303. doi: [10.1016/S0168-9002\(03\)01368-8](https://doi.org/10.1016/S0168-9002(03)01368-8)
- [33] Shibata K, Iwamoto O, Nakagawa T, et al. JENDL-4.0: a new library for nuclear science and engineering. J Nucl Sci Technol. 2011;48:1–30. doi: [10.1080/18811248.2011.9711675](https://doi.org/10.1080/18811248.2011.9711675)
- [34] Furihata S. Statistical analysis of light fragment production from medium energy proton-induced reactions. Nucl Instrum Meth. 2000;B171(3):251–258. doi: [10.1016/S0168-583X\(00\)00332-3](https://doi.org/10.1016/S0168-583X(00)00332-3)
- [35] Boudard A, Cugnon J, David JC, et al. New potentialities of the Liège intranuclear cascade model for reactions induced by nucleons and light charged particles. Phys Rev. 2013;C87(1). doi: [10.1103/PhysRevC.87.014606](https://doi.org/10.1103/PhysRevC.87.014606)
- [36] Nara Y, Otuka H, Ohnishi A, et al. Relativistic nuclear collisions at 10A GeV energies from p+Be to Au+Au with the hadronic cascade model. Phys Rev C. 2000;61(2). doi: [10.1103/PhysRevC.61.024901](https://doi.org/10.1103/PhysRevC.61.024901)
- [37] Allison J, Amako K, Apostolakis J, et al. Recent developments in geant4. Nucl Instrum Meth. 2016; A835:186–225. doi: [10.1016/j.nima.2016.06.125](https://doi.org/10.1016/j.nima.2016.06.125)
- [38] Maekawa F, von MU, Wilson PPH et al. Production of a dosimetry cross section set up to 50 MeV. Proc. 10th International Symposium on Reactor Dosimetry, 1999 Sep. 12–17, Osaka, Japan, American Society for Testing and Materials, 2001:417.
- [39] Lee E, Shigyo N, Kajimoto T et al. Energy spectra of neutrons penetrating concrete and steel shielding blocks from 24 GeV/c protons incident on thick copper target. Nucl Instr Meth. 2021;A998:165189. doi: [10.1016/j.nima.2021.165189](https://doi.org/10.1016/j.nima.2021.165189)